

1 **Amplified role of potential HONO sources in O₃ formation in North China Plain during**
2 **autumn haze aggravating processes**

3 Jingwei Zhang^{1*}, Chaofan Lian^{2,3*}, Weigang Wang^{2,3*}, Maofa Ge^{2,3,7}, Yitian Guo^{1,4}, Haiyan Ran^{1,4}, Yusheng
4 Zhang⁵, Feixue Zheng⁵, Xiaolong Fan⁵, Chao Yan⁶, Kaspar R. Daellenbach⁶, Yongchun Liu⁵, Markku Kulmala^{5,6},
5 Junling An^{1,4,7*}

6 1. State Key Laboratory of Atmospheric Boundary Layer Physics and Atmospheric Chemistry (LAPC), Institute of
7 Atmospheric Physics (IAP), Chinese Academy of Sciences, Beijing 100029, China

8 2. State Key Laboratory for Structural Chemistry of Unstable and Stable Species, Beijing National Laboratory for
9 Molecular Sciences (BNLMS), CAS Research/Education Center for Excellence in Molecular Sciences, Institute of
10 Chemistry, Chinese Academy of Sciences, Beijing 100190, China

11 3. [School of Chemical Sciences, University of Chinese Academy of Sciences, Beijing 100049, China](#)

12 4. [College of Earth and Planetary Sciences, University of the Chinese Academy of Sciences, Beijing 100049,](#)
13 [China](#)

14 5. [Aerosol and Haze Laboratory, Advanced Innovation Center for Soft Matter Science and Engineering, Beijing](#)
15 [University of Chemical Technology, Beijing, 100029, China](#)

16 6. [Institute for Atmospheric and Earth System Research/Physics, Faculty of Science, P.O. Box 64, 00014](#)
17 [University of Helsinki, Helsinki, Finland](#)

18 7. [Center for Excellence in Urban Atmospheric Environment, Institute of Urban Environment, Chinese Academy](#)
19 [of Sciences, Xiamen 361021, China](#)

20 *Corresponding author: Weigang Wang (wangwg@iccas.ac.cn), Junling An (anjil@mail.iap.ac.cn)

21 **These authors contributed equally.

23 **Abstract:**

24 Co-occurrences of high concentrations of PM_{2.5} and ozone (O₃) have been
25 frequently observed in haze aggravating processes in the North China Plain (NCP)
26 over the past few years. Higher O₃ concentrations in hazy days were supposed to be
27 related to nitrous acid (HONO), but the key sources of HONO enhancing O₃ during
28 haze aggravating processes remain unclear. We added six potential HONO sources,
29 i.e., four ground-based (traffic, soil, and indoor emissions, and the NO₂ heterogeneous
30 reaction on ground surface (Het_{ground})) sources, and two aerosol-related (the NO₂
31 heterogeneous reaction on aerosol surfaces (Het_{aerosol}) and nitrate photolysis
32 (Phot_{nitrate})) sources into the WRF-Chem model and designed 23 simulation scenarios

Formatted: Font: 11 pt

Deleted: 6

Deleted: 3

Deleted: 3

Deleted: 4

Deleted: 4

Deleted: 4

Deleted: 5

Deleted: 5

Deleted: 4

Deleted: 4

Deleted: 5

Deleted: 3

Deleted: 6

Formatted: Font: 小五

Deleted: 4

Deleted: 5

Deleted: 6

Formatted: Font: 小五

Deleted: ,

Deleted: and h

Deleted: during

Deleted: , which was explored by us in this study, ,

Deleted: and will be explored in (This studyresearch by using the WRF-Chem model, ...

Deleted: into the WRF-Chem model, which is improved to included ...

Deleted: potential HONO

Deleted: 5

59 [to explore the unclear key sources](#). The results indicate that ground-based HONO
60 sources producing HONO enhancements showed a rapid decrease with height, while
61 the NO+OH reaction and aerosol-related HONO sources decreased slowly with height.
62 Phot_{nitrate} contributions to HONO concentrations enhanced with aggravated pollution
63 levels. ~~The~~ enhanced HONO due to Phot_{nitrate} in hazy days was about ~~ten times~~ larger
64 than in clean days and Phot_{nitrate} dominated ~~daytime~~ HONO sources (~30–70% when
65 the ratio of the photolysis frequency of nitrate (J_{nitrate}) to gas nitric acid (J_{HNO_3}) equals
66 30) at higher layers (>800 m). Compared with that in clean days, the Phot_{nitrate}
67 contribution to the enhanced daily maximum 8-h averaged (DMA8) O₃ was increased
68 by over one magnitude during the haze aggravating process. Phot_{nitrate} contributed
69 only ~5% of the surface HONO in daytime with a $J_{\text{nitrate}}/J_{\text{HNO}_3}$ ratio of 30 but
70 contributed ~30–50% of the enhanced O₃ near the surface in NCP in hazy days.
71 Surface O₃ was dominated by volatile organic compounds-sensitive chemistry, while
72 O₃ at higher altitude (>800m) was dominated by NO_x-sensitive chemistry. Phot_{nitrate}
73 had a limited impact on nitrate concentrations (<15%) even with a $J_{\text{nitrate}}/J_{\text{HNO}_3}$ ratio of
74 120. The above results suggest ~~the potential but significant impact of Phot_{nitrate} on O₃~~
75 ~~formation, and that~~ more ~~comprehensive~~ studies ~~on Phot_{nitrate}~~ in the atmosphere are
76 still needed.

Deleted: ,

Deleted: the

Deleted: one order of magnitude

Formatted: Subscript

Formatted: Subscript

Deleted: field

Deleted: of J_{nitrate}

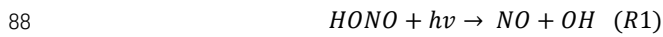
Deleted: nitrate photolysis

Formatted: Subscript

78 1. Introduction

79 Nitrous acid (HONO) is an important source of the hydroxyl radical (OH) through

86 its photolysis (R1), and contributes ~20–80% of the primary OH production (Alicke
87 et al., 2002; Hendrick et al., 2014; Kim et al., 2014).



89 Although it has passed forty years since the first detection of HONO in the
90 atmosphere (Perner and Platt, 1979), the sources of HONO (especially daytime) and
91 the dynamic parameters of HONO formation mechanisms are still not well understood
92 (Ge et al., 2021). The current air quality models with the default gas-phase reaction
93 (the reverse reaction of R1) always severely underestimate HONO observations,
94 resulting in low atmospheric oxidation capacity and underestimation of secondary
95 pollutants like ozone (O₃) (Li et al., 2010, 2011; Sarwar et al., 2008; Zhang et al.,
96 2016, 2019a).

Deleted: ,

Deleted: t

97 HONO sources can be generally classified into three categories, i.e., direct
98 emissions, homogeneous and heterogeneous reactions. Direct emissions are mainly
99 from traffic (Kramer et al., 2020; Kurtenbach et al., 2001; Liao et al., 2021), soil
100 (Kubota and Asami, 1985; Oswald et al., 2013; Wu et al., 2019; Xue et al., 2021),
101 biomass burning (Cui et al., 2021; Rondon and Sanhueza, 1989; Theys et al., 2020)
102 and indoor combustion processes (Klosterkother et al., 2021; Liu et al., 2019; Pitts et
103 al., 1985). The reaction of nitric oxide (NO) with OH (Pagsberg et al., 1997; Stuhl and
104 Niki, 1972) is usually thought as the dominant homogeneous reaction and is important
105 during daytime but could be neglected at night due to low OH concentrations. Other
106 minor homogeneous HONO sources including nucleation of NO₂, H₂O, and NH₃
107 (Zhang and Tao, 2010), via the photolysis of ortho-nitrophenols (Bejan et al., 2006;

Formatted: Subscript

Formatted: Subscript

Formatted: Subscript

110 [Chen et al., 2021; Lee et al., 2016](#)), via the electronically excited NO_2 and H_2O
111 [\(Crowley and Carl, 1997; Dillon and Crowley, 2018; Li et al., 2008\)](#) and via
112 [HO₂·H₂O+NO₂ reaction \(Li et al., 2015; Li et al., 2014; Ye et al., 2015\)](#). The
113 heterogeneous reactions mainly include nitrogen dioxide (NO_2) hydrolysis and
114 reduction reactions on various humid surfaces (Finlayson-Pitts et al., 2003; Ge et al.,
115 2019; Gómez Alvarez et al., 2014; Ma et al., 2013; Marion et al., 2021; Sakamaki et
116 al., 1983; Tang et al., 2017; Yang et al., 2021b) and nitrate photolysis ($\text{Phot}_{\text{nitrate}}$)
117 (Romer et al., 2018; [Ye et al., 2016a, b](#); Zhou et al., 2003), and are usually thought as
118 the main contributors to HONO concentrations in the atmosphere.

119 Among those potential HONO sources, the photolysis of nitrate to produce HONO
120 in the atmosphere has received extensive attention over the past several years, and the
121 $\text{Phot}_{\text{nitrate}}$ frequency (J_{nitrate}) is still argued ([Gen et al., 2022](#)). In the laboratory studies,
122 some researchers (Bao et al., 2018; Ye et al., 2016a, 2017) showed that $\text{Phot}_{\text{nitrate}}$ was
123 an important HONO source, the measured J_{nitrate} was 1–3 orders larger than the J_{gas}
124 nitric acid (HNO_3) photolysis frequency (J_{HNO_3}) and could reach up to 10^{-4} s^{-1} , and a
125 number of substances including humic acid (Yang et al., 2018), sulfate (Bao et al.,
126 2020) and TiO_2 (Xu et al., 2021) might enhance the reaction significantly; while Shi et
127 al. (2021) found that the $J_{\text{nitrate}}/J_{\text{HNO}_3}$ ratio was <10 when using suspended submicron
128 particulate sodium and ammonium nitrate rather than $\text{PM}_{2.5}$ samples. In the field
129 studies combining with model simulations, Kasibhatla et al. (2018) compared NO_x
130 observations in Cape Verde Atmospheric Observatory with GEOS-Chem (Goddard
131 Earth Observing System-Chemistry) model simulations and reported a $J_{\text{nitrate}}/J_{\text{HNO}_3}$

Formatted: Font: 小四, Not Italic, Font color: Text 1

Formatted: Subscript

Formatted: Subscript

Formatted: Subscript

Formatted: Subscript

Formatted: Subscript

Formatted: Subscript

Deleted: nitrate photolysis

Formatted: Subscript

Deleted: (Gen et al., 2022)

Deleted: nitrate photolysis

Formatted: Subscript

Deleted: gaseous

136 ratio of 25–50, Romer et al. (2018) reported a $J_{\text{nitrate}}/J_{\text{HNO}_3}$ ratio of < 30 based on
137 observations of NO_x ($= \text{NO} + \text{NO}_2$) and HNO_3 over the Yellow Sea and a box model
138 simulation, while larger $J_{\text{nitrate}}/J_{\text{HNO}_3}$ ratios (e.g., 300) were inconsistent with the
139 observed NO_x to HNO_3 ratios. Adopting a $J_{\text{nitrate}}/J_{\text{HNO}_3}$ ratio of ~ 120 could greatly
140 improve daytime surface HONO simulations (contributed ~ 30 – 40% of noontime
141 HONO) by using the Community Multiscale Air Quality model (CMAQ) in the Pearl
142 River Delta (Fu et al., 2019) or a box model in the Yangtze River Delta (Shi et al.,
143 2020), while a $J_{\text{nitrate}}/J_{\text{HNO}_3}$ ratio of 30 produced negligible HONO in clean periods
144 ($\sim 2\%$) and slightly higher HONO in heavy haze periods ($\sim 8\%$) in the North China
145 Plain (NCP) by using a box model (Xue et al., 2020) and $\sim 1\%$ by using CMAQ in
146 urban Beijing (Zhang et al., 2021). Recently, Zheng et al. (2020) evaluated the effect
147 of three $J_{\text{nitrate}}/J_{\text{HNO}_3}$ ratios (1, 10 and 100) on heterogeneous sulfate formation by
148 using CMAQ and large uncertainties of simulated sulfate concentrations were
149 reported. The mostly adopted $J_{\text{nitrate}}/J_{\text{HNO}_3}$ ratios were 1–30 or 100–120 with large
150 uncertainties, so more efforts are needed to better understand the $\text{Phot}_{\text{nitrate}}$ impact on
151 atmospheric oxidation capacity and concentrations of HONO and other secondary
152 pollutants.

153 A number of potential HONO sources (e.g., direct emissions, NO_2 heterogeneous
154 reactions and $\text{Phot}_{\text{nitrate}}$) have been coupled into several air quality models (An et al.,
155 2013; Fu et al., 2019; Guo et al., 2020; Li et al., 2010, 2011; Sarwar et al., 2008; Tang
156 et al., 2015; Xu et al., 2006; Zhang et al., 2019a, 2019b, 2020a, 2021, 2022) to
157 improve HONO simulations. The improved HONO sources can produce more OH,

Deleted: was

Deleted:

Formatted: Subscript

Formatted: Subscript

Deleted: model

Deleted: ,

Deleted: of nitrate photolysis

Formatted: Subscript

Deleted: HONO concentrations,

Deleted: concentrations

Deleted: nitrate photolysis

Formatted: Subscript

166 which is favorable for the formation of O₃ (Fu et al., 2019; Guo et al., 2020; Li et al.,
167 2010; Xing et al., 2019; Zhang et al., 2016, 2019a, 2022). O₃ can directly damage
168 plants and threaten human health (Avnery et al., 2011a, b; Feng et al., 2015, 2019,
169 [2022](#); Mills et al., 2007, 2018; Richards et al., 1958; Selin et al., 2009; Wilkinson et
170 al., 2012; [Zhao et al., 2021](#)), an increasing trend of O₃ concentrations in China has
171 been widely reported in recent years (Chen et al., 2020a; Li et al., 2020; Lu et al.,
172 2020; Ma et al., 2016; Maji and Namdeo, 2021), [and](#) made O₃ pollution be a severe
173 concern. A co-occurrence of high PM_{2.5} and O₃ concentrations has been frequently
174 found in China over the past few years, ~~researchers speculated the significant role of~~
175 HONO in producing O₃ enhancements (Feng et al., 2021; Fu et al., 2019; Tie et al.,
176 2019; Yang et al., 2021a). ~~Nevertheless, the current knowledge on the HONO~~
177 ~~difference in O₃ formation during clean and hazy days is still unclear, especially the~~
178 relative contribution of each potential HONO source to O₃ enhancements during haze
179 aggravating processes with a co-occurrence of high PM_{2.5} and O₃ concentrations.

180 In this study, time series of pollutants including HONO, O₃, and nitrate were
181 collected in NCP in Oct.11–31 of 2018, in which high concentrations of PM_{2.5}
182 accompanying by high O₃ concentrations were found at least twice in haze events.
183 ~~The specific role of each of potential HONO sources in O₃ formation will be explored~~
184 during these haze events ~~by coupling these potential HONO sources into the Weather~~
185 ~~Research and Forecasting model with Chemistry (WRF-Chem).~~ The relative
186 contribution of each potential HONO source to surface-averaged and
187 vertically-averaged concentrations of HONO and O₃ will be quantified and the

Deleted: and

Deleted:),

Deleted: but

Deleted: and

Deleted: is still unknown to the best of our knowledge

Deleted: ,

Deleted: thus t

Deleted: coupled into the Weather Research and Forecasting model with Chemistry (WRF-Chem) ...

197 uncertainty in key potential HONO sources (e.g., J_{nitrate}) will be discussed, in order to
198 find the key HONO sources resulting in O_3 enhancements in NCP in different
199 pollution levels (especially during haze aggravating processes).

200 2. Data and methods

201 2.1 Observed data

202 The field observation was carried out during October 11–31, 2018, and the
203 observation site was located in the west campus of Beijing University of Chemical
204 Technology (BUCT, 116°18'37" E, 39°56'56" N) in Beijing. BUCT is an urban site
205 close to the third ring road of Beijing, with large human activities, including vehicle
206 emissions. Instruments were set on the 5th floor of the main teaching building. HONO
207 was measured with a home-made water-based long-path absorption photometer (Chen
208 et al., 2020b). A dual-channel absorption system was deployed to subtract the
209 potential interferences, e.g., NO_2 hydrolysis. A set of on-line commercial analyzers
210 (Thermo 48i, 42i, 49i, 43i) was used for measurements of CO , NO_x , O_3 , and SO_2 . To
211 be specific, the 42i used molybdenum NO_2 -to- NO converter, there would be a NO_2
212 overestimation for the conversion of HONO, HNO_3 , or other NO_y . Considering the
213 relatively lower concentration compared with NO_2 , the impact would be minor. The
214 chemical composition of $\text{PM}_{2.5}$ was analyzed with a Time-of-Flight Aerosol Chemical
215 Speciation Monitor (ToF-ACSM, Aerodyne). ToF-ACSM was developed via Fröhlich
216 et al. (2013) for Non-refractory $\text{PM}_{2.5}$ measurement. The detailed usage could be
217 found in Liu et al. (2020), where ionization efficiency calibration of nitrate was

Formatted: Superscript

Formatted: Subscript

Formatted: Subscript

Formatted: Subscript

Formatted: Subscript

Formatted: Subscript

Deleted:

Formatted: Subscript

Formatted: Subscript

219 performed using 300 nm dry NH₄NO₃ every month during the observation. An online
220 Single Photon Ionization Time-of-Flight Mass Spectrometer (SPI-ToF-MS, Hexin)
221 was used for the detection of a large variety of volatile organic compounds (VOCs)
222 (Gao et al., 2013). Surface observations of O₃, NO₂, PM_{2.5} and PM₁₀ at 95 sites in
223 NCP were obtained from <https://quotsoft.net/air/>, issued by the China Ministry of
224 Ecology and Environment; surface meteorological observations at 284 sites in NCP
225 were taken from the National Climatic Data Center, China Meteorological
226 Administration (**Fig.1**).

Formatted: Subscript

Formatted: Subscript

227 The vertical HONO observations were not available during the Oct.11–31 of 2018
228 at the BUCT site, we used the observed vertical HONO concentrations from Meng et
229 al. (2020) in urban Beijing in December of 2016 to evaluate our simulation of vertical
230 HONO concentrations, which were also used by Zhang et al. (2021) in their CMAQ
231 evaluation.

Deleted: was

Deleted: at

Deleted: validate

Deleted: model validation

233 **2.2 Model description**

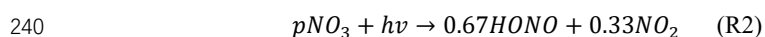
Formatted: Font: (Default) Times New Roman, 小四, Bold, Font color: Text 1

234 The improved WRF-Chem (version 3.7.1), which contained six potential HONO
235 sources, i.e., traffic (E_{traffic}), soil (E_{soil}), and indoor (E_{indoor}) emissions, Phot_{nitrate} in the
236 atmosphere, and NO₂ heterogeneous reactions on aerosol (Het_{aerosol}) and ground
237 (Het_{ground}) surfaces (Zhang et al., 2019a), was used in this study. Phot_{nitrate} was newly
238 added in WRF-Chem (R2) following the work of Fu et al. (2019), Ye et al. (2017),
239 and Zhou et al. (2003):

Deleted: nitrate photolysis

Formatted: Subscript

Deleted: (Phot_{nitrate})



247 For $Het_{aerosol}$ and Het_{ground} , laboratory studies suggest that these heterogeneous
 248 reactions of NO_2 to HONO are first order in NO_2 (Aumont et al., 2003;
 249 Finlayson-Pitts et al., 2003; Saliba et al., 2000):

Formatted: Not Superscript/ Subscript

Formatted: Indent: First line: 0.63 cm

Deleted: ed

Formatted: Subscript

Deleted: is

Formatted: Subscript



252 The first-order rate constants for aerosol (k_a) and ground (k_g) surface reactions
 253 are calculated below:

Deleted: t

Formatted: Indent: First line: 0.63 cm

254 $k_a = \frac{1}{4} \times v_{NO_2} \times \left(\frac{S}{V}\right) \times \gamma$ (E1)

Formatted: Centered

Formatted: Font: Not Italic

255 $k_g = \frac{f \times v_d}{H}$ (E2)

Formatted: Font: Italic

256 where v_{NO_2} is the mean molecular speed of NO_2 , $\frac{S}{V}$ is the surface to volume ratio for
 257 aerosols, γ is the reactive uptake coefficient of aerosols, f is the proportion of
 258 deposited NO_2 reaching the surface in participating HONO formation, v_d is the dry
 259 deposition velocity of NO_2 , and H is the first model layer height above the ground
 260 (~35 m). It should be noted that not 100% (50% is commonly accepted) of the
 261 participated NO_2 could be converted to HONO in R3 and R4, so k_a and k_g were
 262 multiplied by 0.5 in the final calculation of HONO heterogeneous formation via NO_2 .

Deleted: in which

Deleted: W

Formatted: Subscript

Deleted: the

Formatted: Subscript

Formatted: Subscript

Deleted: is the

263 The two factors γ and f were improved from previous studies (Li et al., 2010; Liu
 264 et al., 2014; Zhang et al., 2019a) and calculated by:

Deleted: a production rate of 50% is commonly accepted, and the ...

Deleted: y

Deleted: for

Formatted: Subscript

Deleted: The uptake coefficient (γ) of NO_2 on aerosol surfaces, and the yield (f) of HONO from NO_2 reaching the ground surfaceThe

265 $\gamma = 5 \times 10^{-6} \times \left(1 + \frac{SR}{\alpha}\right)$ (E3)

Deleted: R3

266 $f = 0.08 \times \left(1 + \frac{SR}{\alpha}\right)$ (E4)

Deleted: R4

267 where SR denotes solar radiation ($W m^{-2}$), α is an adjusted parameter and set as 100
 268 ($W m^{-2}$), thus γ and f became continuous functions during the whole day (γ and f

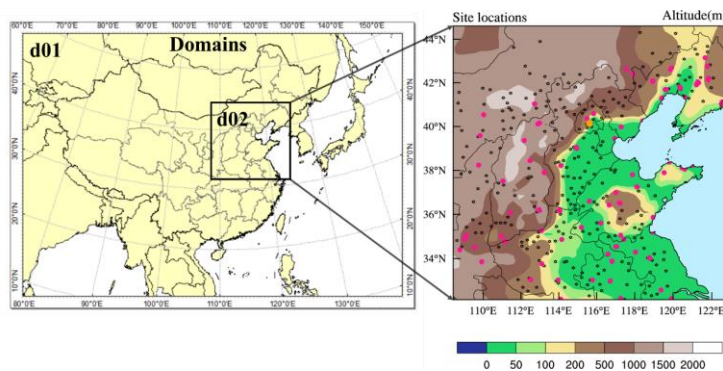
Formatted: Superscript

285 enhanced by ten times and reached 5×10^{-5} and 0.8 when SR reached 900 W m^{-2} at
286 noontime, respectively).

Deleted: one order of magnitude

Deleted:

287 The physical and chemical schemes used in this study are given in **Table 1**. Two
288 domains were adopted, domain one contains 82×64 grid cells with a horizontal
289 resolution of 81 km, domain two contains 51×51 grid cells with a horizontal
290 resolution of 27 km (**Fig.1**), both with 17 vertical layers encompassing from the
291 surface to 100 hPa. The observational sites are shown in the right panel of **Fig.1**,
292 including one HONO observation site (the orange dot in urban Beijing), 95
293 observation sites of $\text{PM}_{2.5}$, NO_2 and O_3 (pink dots) and 284 meteorological monitoring
294 sites (black dots).



295
296 **Figure 1** Domains of WRF-Chem used in this study (left panel), and the locations of one HONO
297 observation site (the orange dot in urban Beijing), 95 environmental monitoring ($\text{PM}_{2.5}$, NO_2 and
298 O_3) sites (deep pink dots), and 284 meteorological observation sites (black dots) in domain 2 (right
299 panel).

300

301 The anthropogenic emissions in East Asia in 2010 were taken from the MIX

304 emission inventory (Li et al., 2017) (<http://www.meicmodel.org/>), including both
305 gaseous and aerosol species, i.e., SO₂, NO_x, CO, VOCs, NH₃, PM₁₀, PM_{2.5}, BC, OC
306 and CO₂, and were provided monthly by five sectors (power, industry, residential,
307 transportation, and agriculture) at a resolution of 0.25° × 0.25°. VOC emissions were
308 speciated into model-ready inputs according to the MOZART chemical mechanism to
309 build the WRF-Chem emission files. The anthropogenic emissions in China were
310 replaced by employing the MEIC 2016 (the Multi-resolution Emission Inventory for
311 China) developed by Tsinghua University. The NH₃ emissions in China were from
312 Dong et al. (2010), biomass burning emissions were from Huang et al. (2012) and
313 biogenic emissions were calculated using the Model of Emissions of Gases and
314 Aerosols from Nature (MEGAN) (Guenther et al., 2012). Due to the sharp reduction
315 of anthropogenic emissions in recent years, the default emission inventory was
316 systematically overestimated in autumn of 2018, especially for SO₂ and PM_{2.5}
317 concentrations. Based on the comparison of simulations and observations (the urban
318 Beijing site plus other 95 pollutant monitoring sites in NCP), we cut off 80% of SO₂
319 emissions, 50% of NH₃ emissions, 30% of toluene emissions, and 50% of PM_{2.5} and
320 PM₁₀ emissions. The cut-off emissions are largely close to the emission reductions in
321 east China during 2013 to 2017 (Zhang and Geng, 2019). The revised emissions
322 significantly improved regional PM_{2.5} simulations in NCP (**Fig.S1**), and the
323 simulations of gases and PM_{2.5} in urban Beijing (**Fig.S2**).

324 The National Centers for Environmental Prediction (NCEP) 1° × 1° final
325 reanalysis data (FNL) (<https://rda.ucar.edu/datasets/ds083.2/>) were used in this study

326 to obtain the meteorological initial and boundary conditions every 6 h. The global
 327 simulations of MOZART-4 (<https://www.acom.ucar.edu/wrf-chem/mozart.shtml>)
 328 were used as the chemical initial and boundary conditions (every 6 h).

329

330 **Table1** Physical and chemical options in WRF-Chem used in this study

Options	WRF-Chem
Advection scheme	Runge-Kutta 3 rd order
Boundary layer scheme	YSU
Cloud microphysics	Lin et al. (1983)
Cumulus parameterization	New Grell scheme
Land-surface model	Noah
Long-wave radiation	RRTM
Short-wave radiation	Goddard
Surface layer	Revised MM5 Monin-Obukhov scheme
Aerosol option	MOSAIC (Zaveri et al., 2008)
Chemistry option	Updated MOZART mechanism (Emmons et al., 2010)
Photolysis scheme	F-TUV

331

332 Totally 23 simulation scenarios were performed in this study (**Table 2**), in which
 333 the base case only considered the default homogeneous reaction ($\text{OH} + \text{NO} \rightarrow$
 334 HONO), case 6S contained six potential HONO sources while case A, B, C, D, E and
 335 F contained each of the six potential HONO sources, respectively. Other 15 cases
 336 (A_double, A_half, ..., Nit_120, D_NO₂ and D_HONO) were used to evaluate the
 337 uncertainties of the six potential HONO sources (**Table 2**). All of the cases were
 338 simulated with a spin-up of 7 days. J_{nitrate} and J_{HNO_3} denote the photolysis frequency of
 339 nitrate and gas nitric acid in the atmosphere, respectively. ~~The~~ enhancement factor for
 340 F_double was 1.25 rather than 2.0 to avoid the production rate of HONO from NO₂
 341 reaching the surface exceeding 100%. ~~The~~ 0.33NO₂ in D NO₂ or 0.67HONO in
 342 D_HONO referred to the assumed $\text{Phot}_{\text{nitrate}}$ products in R2.

Formatted: Superscript

Deleted: ;

Deleted: the

Deleted: %,

Deleted: while

Formatted: Subscript

Deleted: of the nitrate photolysis

Deleted: The c

349

350 **Table 2.** Simulation scenarios designed in this study.

Case	HONO sources
Base	Default (OH + NO → HONO)
6S	Default + E _{traffic} + E _{soil} + E _{indoor} + Phot _{nitrate} (J _{nitrate} /J _{HNO3} = 30) + Het _{aerosol} + Het _{ground}
A	Default + E _{traffic}
B	Default + E _{soil}
C	Default + E _{indoor}
D	Default + Phot _{nitrate} (J _{nitrate} /J _{HNO3} = 30)
E	Default + Het _{aerosol}
F	Default + Het _{ground}
A_double	----- Default + 2×E _{traffic}
A_half	Default + 0.5×E _{traffic}
B_double	Default + 2×E _{soil}
B_half	Default + 0.5×E _{soil}
C_double	Default + 2×E _{indoor}
C_half	Default + 0.5×E _{indoor}
E_double	Default + Het _{aerosol} (2×γ)
E_half	Default + Het _{aerosol} (0.5×γ)
F_double	Default + Het _{ground} (1.25×f)
F_half	Default + Het _{ground} (0.5×f)
Nit_1	Default + Phot _{nitrate} (J _{nitrate} /J _{HNO3} = 1)
Nit_7	Default + Phot _{nitrate} (J _{nitrate} /J _{HNO3} = 7)
Nit_120	Default + Phot _{nitrate} (J _{nitrate} /J _{HNO3} = 120)
D_NO2	Only 0.33NO ₂ produced in Phot _{nitrate} for case D
D_HONO	Only 0.67HONO produced in Phot _{nitrate} for case D

351 **3.Results**

352 **3.1 Comparison of simulations and observations**

353 **3.1.1 Meteorological factors**

354 The statistical metrics of simulated meteorological parameters at 284 sites in NCP
 355 including air temperature (T), relative humidity (RH) and wind speed (WS) were
 356 comparable with the previous modelling results of other researchers (Table 3). The
 357 simulated wind direction (WD) bias within 45° accounted for ~56%, and the bias
 358 within 90° accounted for ~80%, suggesting that the simulated WD captured the main
 359 observed WD.

Deleted: ,

Deleted: the

362

363 **Table 3.** Performance metrics (index of agreement (IOA), RMSE (root-mean-square error)
364 and MB (mean bias)) of WRF-Chem simulated air temperature, relative humidity, wind speed and
365 direction at 284 meteorological sites in the North China Plain during Oct. 11–31 of 2018. The
366 definitions of the metrics used in this study are given in Text S1.

Deleted: is

	IOA	RMSE	MB	Reference
T (°C)	0.97	1.4	-1.1	This work
	0.90	2.5	0.2	(Wang et al., 2014)
	0.90	/	-0.9	(Wang et al., 2010)
	0.88	/	0.5	(Li et al., 2012)
	/	3.1	0.8	(Zhang et al., 2012)
RH (%)	0.90	9.0	-7.1	This work
	0.78	16.3	-5.5	(Wang et al., 2014)
	0.78	/	-1.3	(Wang et al., 2010)
	0.86	/	-1.1	(Li et al., 2012)
	/	17.4	-5.7	(Zhang et al., 2012)
WS (m s⁻¹)	0.48	1.4	1.3	This work
	0.56	2.5	1.6	(Wang et al., 2014)
	0.65	2.1	0.9	(Wang et al., 2010)
	0.62	1.5	0.6	(Li et al., 2012)
	/	2.2	1.1	(Zhang et al., 2012)
WD Bias	<i>0-45°</i>	<i>45-90°</i>	<i>>90°</i>	
Count	<i>75701</i>	<i>21500</i>	<i>28075</i>	<i>135276(Total)</i>
Percentage	55.96%	23.29%	20.75%	

367 3.1.2 Pollutant concentrations at the BUCT site

368 Time series of the observational data at the BUCT site are shown in Fig.2, the
369 gray shaded periods stand for three haze aggravating processes, while the cyan shaded
370 period denotes typical clean days, respectively. The hourly largest observations of O₃
371 (~50–75 ppb) and PM_{2.5} (~100–200 µg/m³) were both relatively higher in hazy days
372 than in clean days, especially for the first two haze events (the O₃ concentrations in
373 the third haze event was relatively lower due to the higher NO_x concentrations in the
374 urban area).

375 The observed PM_{2.5} and nitrate trends at the BUCT site were well simulated

377 (Fig.2a&b), and NO₂ simulations generally agreed with the observations (Fig.2c).

378 The promotion effect of the six potential HONO sources on the formation of
379 secondary aerosols leads to an increase in concentrations of PM_{2.5} and nitrate for case
380 6S, despite nitrate consumption through Phot_{nitrate} (Li et al., 2010; Qu et al., 2019; Fu
381 et al., 2019; Zhang et al., 2019a, 2021), detailed nitrate variation caused by each of
382 the six potential HONO sources in case 6S is presented in Fig.S3. The overestimation
383 of nitrate could be partially caused by the uncertainties in the anthropogenic emission
384 inventory, e.g., the overestimation of NO_x emissions (Fig.2c). The inadequate
385 understanding of the nitrate formation mechanism could also be related to nitrate
386 simulation bias, which was also found in some related studies using CMAQ (Fu et al.,
387 2019; Zhang et al., 2021).

388 Hourly and diurnal HONO simulations at the BUCT site (Fig.2d&3a) were
389 significantly improved in the 6S case (mean is 1.47 ppb) compared with the base case
390 (mean is 0.05 ppb). The normalized mean bias (NMB) was remarkably reduced to
391 -14.22% (6S) from -97.11% (Base), and the index of agreement (IOA) was improved
392 significantly to 0.80 (6S) from 0.45 (Base), (Fig.2d). The underestimation of the
393 simulated HONO (6S) on Oct.15 and Oct.22 was mainly caused by the earlier
394 scavenging of pollutants at the BUCT site in the used model (Fig.2a&d),

395 As for O₃, noticeable improvements could be found at the BUCT site after
396 considering the six potential HONO sources, especially in hazy days (Fig.2e&f). The
397 mean bias (MB) was improved to -3.61 ppb (6S) from -7.09 ppb (Base), and the IOA
398 was improved to 0.86 (6S) from 0.78 (Base), (Fig.2e). Specially, the 6S case

Deleted: The increased PM_{2.5} and nitrate concentrations for 6S case was because of the ...

Deleted: additional

Deleted: formation

Formatted: Subscript

Deleted: the

Deleted: of nitrate

Deleted: nitrate photolysis

Formatted: Subscript

Deleted: given

Formatted: Font: Bold

Formatted: Subscript

Formatted: Font: Bold

Deleted: 0.86 (6S) from 0.78 (Base)

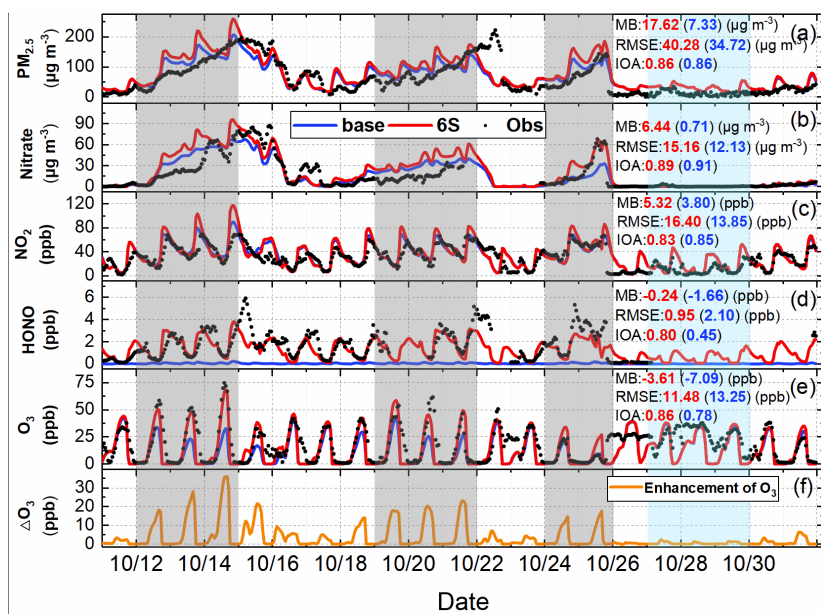
Formatted: Font: Bold

Deleted: .

Deleted: 0.80 (6S) from 0.45 (Base)

410 significantly enhanced daytime hourly O_3 by 15–35 ppb compared with the base case
 411 and the simulated O_3 was very close to the observations in hazy days (**Fig.2e**). Larger
 412 daytime O_3 enhancements were accompanied with higher $PM_{2.5}$ concentrations during
 413 haze aggravating processes, while in clean days the daytime enhanced O_3 due to the
 414 potential HONO sources was mostly < 5 ppb (**Fig.2e&f**). The diurnal O_3 pattern
 415 during the first two haze aggravating processes is presented in **Fig.3b**, significant
 416 improvements in daily maximum 8-h (10:00–17:59) averaged (DMA8) O_3 (18.8 ppb)
 417 occurred at the BUCT site after considering the six potential HONO sources, and the
 418 NMB of DMA8 O_3 was remarkably improved to -2.38% (6S) from -47.14% (Base).

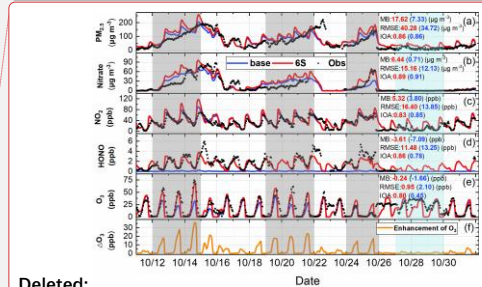
419



420

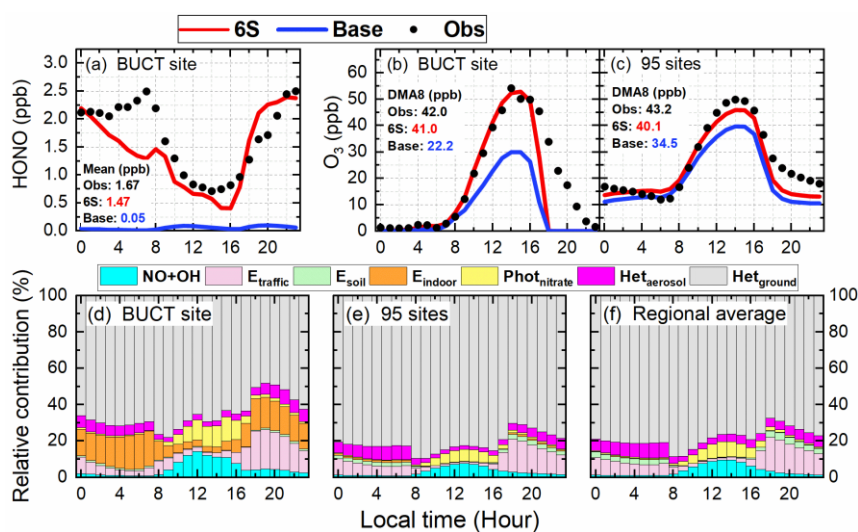
421 **Figure 2** Comparison of simulated (Base and 6S cases) and observed hourly concentrations of
 422 $PM_{2.5}$, nitrate, NO_2 , HONO and O_3 (a–e), and the hourly enhanced concentrations of O_3 (ΔO_3) (f)

Commented [j1]: The statistics for O_3 and HONO was opposite in the original figure, which is corrected now. For the orders of panel O_3 and HONO was swapped previously to let O_3 next to ΔO_3 , but the statistics was forgotten to change the orders simultaneously.



Deleted:

424 caused by the six potential HONO sources (6S minus Base) at the BUCT site during Oct.11–31 of
 425 2018.
 426
 427



428
 429 **Figure 3** Comparison of diurnal mean simulations (Base and 6S cases) and observations of
 430 HONO during the study period (a) and O₃ during the first two haze events at the BUCT site (b),
 431 and O₃ averages at the 95 NCP monitoring sites during the study period (c); and the relative
 432 contributions of each of the six potential HONO sources and the reaction of OH with NO to
 433 surface HONO concentrations for the 6S case at the BUCT site (d), at the 95 monitoring sites (e)
 434 and in the whole NCP region (f). (The calculated 24-h mean HONO concentrations and DMA8 O₃
 435 concentrations were given in panels (a) – (c)).

436
 437 The relative contribution of each HONO source near the surface at the BUCT site
 438 for the 6S case is shown in **Fig.3d**. Briefly, Het_{ground} was the largest source during

Deleted: .

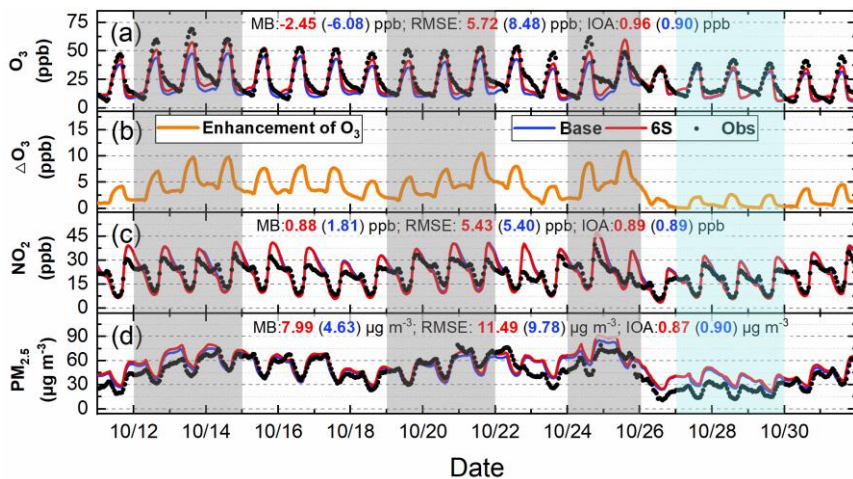
Formatted: Font: Not Bold

440 daytime and nighttime (~50–70%), consistent with the results of Zhang et al. (2021).
441 $\text{Phot}_{\text{nitrate}}$ ($J_{\text{nitrate}}/J_{\text{HNO}_3} = 30$) and the NO+OH reaction contributed similarly ~1–12%
442 during daytime. E_{traffic} was important during nighttime (~10–20%) but small during
443 daytime (<5%). The contribution of $\text{Het}_{\text{aerosol}}$ to HONO concentrations was minor
444 (~2–3%) in daytime and ~6–10% in nighttime. E_{soil} could be neglected while the
445 contribution of E_{indoor} was close to that of E_{traffic} in urban Beijing. The relative
446 contribution of the potential HONO sources in this study was comparable with the
447 result of Fu et al. (2019) by using CMAQ, except for the contribution of $\text{Phot}_{\text{nitrate}}$ due
448 to the different $J_{\text{nitrate}}/J_{\text{HNO}_3}$ ratios (30 in our study and ~120 in Fu et al. (2019)).
449

450 3.1.3 Pollutant concentrations in NCP

451 The 95-site-averaged hourly simulations and observations of O_3 , NO_2 and $\text{PM}_{2.5}$
452 during the study period are shown in **Fig.4**. The six potential HONO sources
453 significantly improved hourly O_3 simulations, remarkably enhanced the daily
454 maximum O_3 by ~5–10 ppb during Oct. 11–25, and by ~2–4 ppb during Oct. 26–31
455 (**Fig.4a&b**). The simulations of NO_2 well agreed with the observations, and the mean
456 concentrations were 22.55 (Base), 21.62 (6S) and 20.74 (Obs) ppb (**Fig.4c**). The
457 $\text{PM}_{2.5}$ simulations generally followed the observed $\text{PM}_{2.5}$ trend but were
458 overestimated by ~8 $\mu\text{g m}^{-3}$, with averaged concentrations of 49.94 (Base), 53.30 (6S)
459 and 45.31 (Obs) $\mu\text{g m}^{-3}$ (**Fig.4d**), respectively.

460



461

462 **Figure 4** Comparison of 95-site-averaged hourly simulations (Base and 6S cases) and observations of

463 O₃(a), NO₂ (c) and PM_{2.5} (d), and O₃ enhancements due to the six potential HONO sources (6S minus

464 Base case) (b) in the North China Plain during Oct.11–31 of 2018.

465

466 The 95-site-averaged diurnal simulations and observations of O₃ are presented in

467 **Fig.3c**, O₃ simulations showed a remarkable improvement when the six potential

468 HONO sources were considered, the six potential HONO sources produced a mean

469 enhancement of 5.7 ppb in DMA8, O₃ and improved the NMB to -7.16% from -20.32%

470 at the 95 sites in NCP. The 95-site-averaged diurnal simulations and observations of

471 NO₂ and PM_{2.5} during the study period are demonstrated in **Fig.S4**. NO₂ simulations

472 generally followed the observed trend but were underestimated during 04:00 to 16:00

473 and overestimated after 18:00 (**Fig.S4a**), PM_{2.5} simulations agreed with the observed

474 diurnal pattern but were overestimated for both cases during the whole day (**Fig.S4b**).

475 The relative contribution of each HONO source near the surface at the 95 NCP

476 sites for the 6S case is shown in **Fig.3e**. Het_{ground} was the dominant source during

Deleted: mean

Deleted: simulated

Deleted: observed hourly

Deleted: (10:00–17:59)

Deleted: from -20.32%

Deleted: S3

Deleted: S3a

Deleted: S3b

Formatted: Font: 小四

Deleted: thus the results of the 95 sites

Deleted: S4

Deleted: ly

485 daytime and nighttime (~70–80%). $Phot_{nitrate}$ ($J_{nitrate}/J_{HNO_3} = 30$) and the NO+OH
486 reaction nearly equaled and contributed ~2–8% during daytime (~5% on average).
487 $E_{traffic}$ was important during nighttime (~10–15%) but small during daytime (<3%).
488 The contribution of $Het_{aerosol}$ to HONO concentrations was <3% in daytime and <10%
489 in nighttime. E_{soil} contributed ~3% in nighttime but could be neglected in daytime.
490 The contribution of E_{indoor} was too small to be noticed at the 95 NCP sites, implying
491 that this source was noticeable only in megacities. The relative contribution of each
492 HONO source in the whole NCP region (all grid cells in domain two except for the
493 seas) is presented in **Fig.3f**, the results were quite similar with those at the 95 sites
494 (**Fig.3f**), [which](#) were representative for the whole NCP region. To further understand
495 the role of potential HONO sources in haze aggravating processes in regional O₃
496 concentrations, the 95 site-averaged surface/vertical HONO concentrations and their
497 impacts during a typical haze event (Oct. 19–21) and a clean period (Oct. 27–29) were
498 analyzed and [are](#) shown in the following sections.

499

500 3.2 Spatial distribution of enhanced DMA8 O₃ by potential HONO sources

501 3.2.1 General patterns of enhanced DMA8 O₃

502 **Fig.S5** shows surface-averaged and zonal-averaged DMA8 O₃ enhancements due
503 to the six potential HONO sources in NCP during the study period (Oct.11-31) and
504 three haze events (Oct.12–14, Oct.18–21 and Oct.24–25). The overall surface DMA8
505 O₃ enhancement decreased gradually from south (6–10 ppb) to north (2–6 ppb)

509 (Fig.S5a) and could reach 10–20 ppb under unfavorable meteorological conditions
510 during haze events (Fig.S5b–d). For the first two haze events, the anti-cyclone in the
511 Shandong peninsula carried pollutants being transported from the southeastern NCP
512 to the western (108–112°E) and northern (39–41°N) NCP, and the six potential
513 HONO sources led to a DMA8 O₃ enhancement of 10–20 ppb (Fig.S5b) and 10–15
514 ppb (Fig.S5c) in Beijing, respectively. For the third haze event, two air masses were
515 converged to form a transport channel from south to north, the O₃ enhancement
516 caused by the six potential HONO sources can reach 10–18 ppb in the southern NCP
517 and decreased to 6–10 ppb in the northern NCP along the transport channel. Vertically,
518 the DMA8 O₃ enhancements were 2–8 ppb during the whole period (Fig.S5e) and
519 increased to 6–12 ppb in these haze events (Fig.S5f–h). The enhanced O₃ near the
520 surface (0–100 m) was slightly smaller than that at higher altitude (Fig.S5f–h), due
521 mainly to the stronger titration of O₃ by NO near the surface. The above results
522 demonstrated that the six potential HONO sources significantly enhanced surface and
523 vertical O₃ concentrations in NCP, especially during haze events.

Deleted: S4a

Deleted: S4b

Deleted: S4b

Deleted: S4c

Deleted: S4e

Deleted: S4f

Deleted: S4f

524

525 3.2.2 During a typical haze aggravating process and a clean period

526 Fig.5 demonstrates surface-averaged and zonally-averaged DMA8 O₃
527 enhancements due to the six potential HONO sources in NCP during a typical haze
528 aggravating process (Oct.19–21, 2018) and a clean period (Oct.27–29, 2018). The
529 increasing trend of DMA8 O₃ enhancements can be clearly seen from Oct.19 to

537 Oct.21 near the surface and in the vertical direction. During the haze aggravating
 538 process, the surface DMA8 O₃ enhancements were ~2–10 ppb (Oct.19), ~6–12 ppb
 539 (Oct.20) and ~8–15 ppb (Oct.21), respectively. ~~the~~ the vertical DMA8 O₃ enhancements
 540 were ~4–7 ppb (Oct.19), ~6–10 ppb (Oct.20), and ~8–15 ppb (Oct.21), respectively. ~~the~~
 541 While during clean days, the surface/vertical DMA8 O₃ enhancements were usually
 542 <4 ppb. The six potential HONO sources significantly enhanced surface and vertical
 543 O₃ concentrations in NCP during haze aggravating processes, the detailed role of the
 544 potential HONO sources on vertical HONO concentrations and their impacts are
 545 presented in the next section.

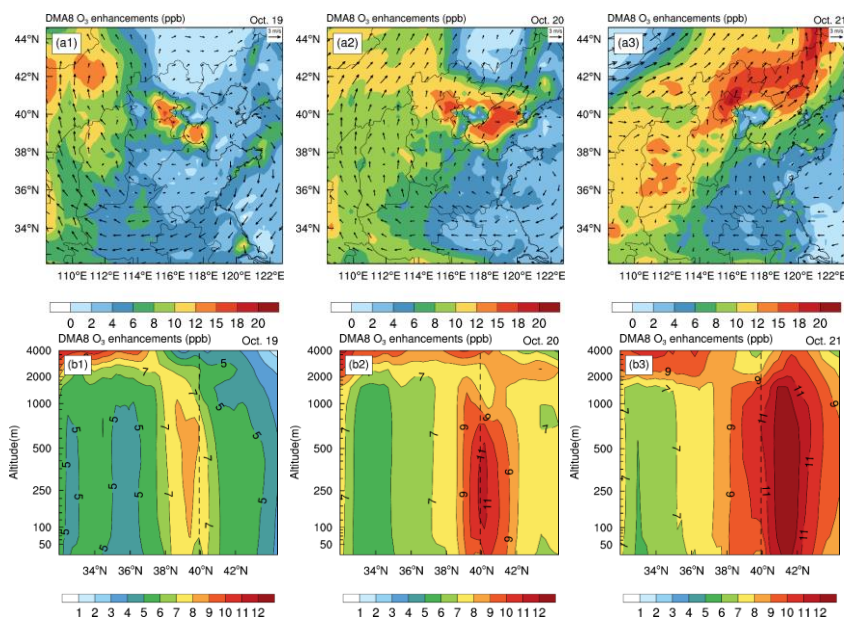
Deleted: , and

Deleted: ;

Deleted: while

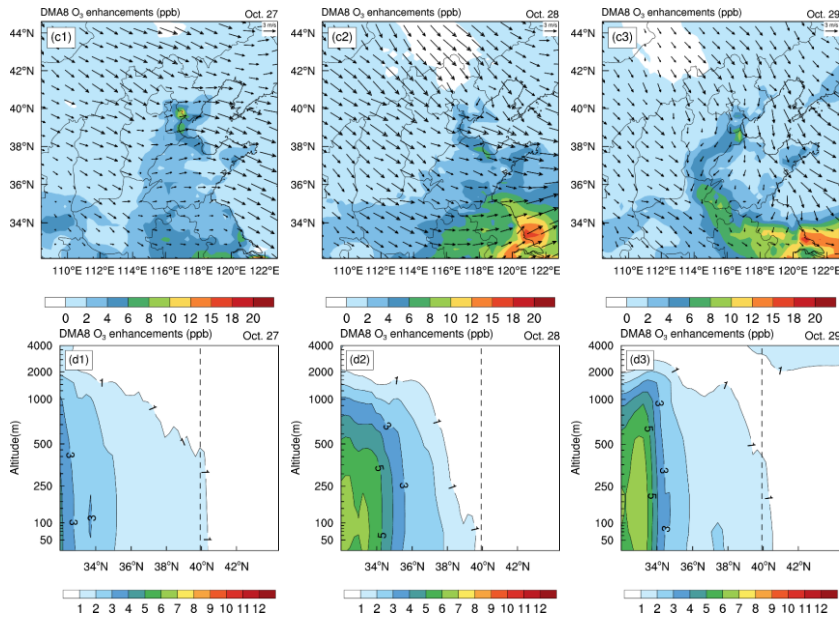
Deleted: were given

546



547

548



553

554

555

556

557

558

559

560

561

562

563

564

565

Figure 5 Surface-averaged (a1–a3, c1–c3) and zonal-averaged (b1–b3, d1–d3) DMA8 O₃ enhancements due to the six potential HONO sources in the North China Plain during a typical haze aggravating process (Oct.19–21, 2018) and a clean period (Oct.27–29, 2018). (The dashed line denotes the latitude of the BUCT site).

Deleted: ly

Deleted: .

3.3 Vertical variations of the six potential HONO sources and their impacts

3.3.1 Six potential HONO sources and their impacts on HONO concentrations

Deleted: Potential

A number of studies have conducted vertical HONO observations abroad (Kleffmann et al., 2003; Ryan et al., 2018; Sorgel et al., 2011; VandenBoer et al., 2013; Villena et al., 2011; Wang et al., 2020; Wong et al., 2011, 2012; Zhang et al., 2009) and in China (Meng et al., 2020; Wang et al., 2019; Xing et al., 2021; Zhu et al., 2011).

Deleted:),

570 A decreasing trend of HONO with height was mostly observed among these studies,
571 and our simulations also reproduced this vertical variation and were comparable with
572 another model simulation by Zhang et al. (2021) who used CMAQ (Fig.S6). For a
573 deep understanding of the role of each considered HONO source in HONO
574 concentrations at different heights, we assessed the contributions of each potential
575 HONO source to HONO concentrations at different heights (Fig.6) during Oct.11–31
576 of 2018.

Deleted: a

Deleted: whom using the

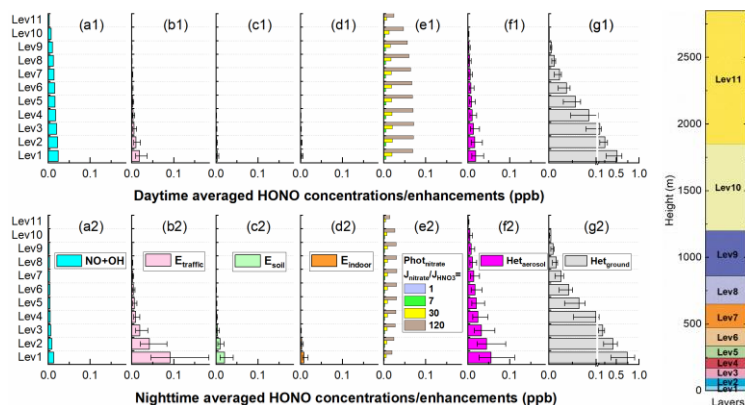
Deleted: model

Deleted: S5

577 Generally, the impacts of ground-based potential HONO sources (E_{traffic} , E_{soil} ,
578 E_{indoor} and H_{etground}) on HONO concentrations decreased rapidly with height, while
579 the NO+OH reaction and aerosol related HONO sources ($Phot_{\text{nitrate}}$ and $H_{\text{et aerosol}}$)
580 decreased slowly with height (Fig.6). During daytime the NO+OH reaction, $Phot_{\text{nitrate}}$
581 and H_{etground} were the three main HONO sources, while during nighttime E_{traffic} ,
582 $H_{\text{et aerosol}}$ and H_{etground} were the three main contributors to HONO concentrations
583 (Fig.6). The HONO concentrations via the NO+OH reaction and $Phot_{\text{nitrate}}$ were
584 higher during daytime. The impact of E_{soil} in the NCP was small, nevertheless, Xue et
585 al. (2021) found strong soil HONO emissions in NCP agricultural fields after
586 fertilization, suggesting that this source may have a remarkable enhancement on
587 regional HONO and secondary pollutants in crop growing seasons.

Deleted: however

588



594
 595 **Figure 6** The 95-site-averaged daytime/nighttime HONO concentrations/enhancements at
 596 different heights when the NO+OH reaction (a1&a2) and each of the six potential HONO sources
 597 (b1–g1&b2–g2) were considered during Oct.11–31 of 2018. (The error bar denotes the
 598 uncertainties of each potential HONO source in HONO concentrations (Table 2). The right panel
 599 denotes the approximate height of each vertical layer above the ground).

Deleted: ,
 Deleted: the

600
 601 The comparison of HONO concentrations/enhancements during a haze
 602 aggravating process and a clean period is shown in Figs.7&8. Generally, daytime
 603 HONO concentrations increased in haze aggravating processes and were higher than
 604 those in clean days. Het_{ground} was the dominant source of the surface HONO in both
 605 hazy and clean days and contributed 80–90% of daytime averaged HONO
 606 concentrations (Fig.8), however, this reaction occurred only on the ground surface,
 607 thus its relative contribution decreased with height, especially in haze aggravating
 608 processes (Fig.8). Although the contribution of the NO+OH reaction to daytime
 609 HONO was small near the surface, its relative contribution to HONO increased with
 610 height, especially in clean days (Fig.8). As for Phot_{nitrate}, a much larger enhancement

Deleted: was
 Deleted: in the first model layer

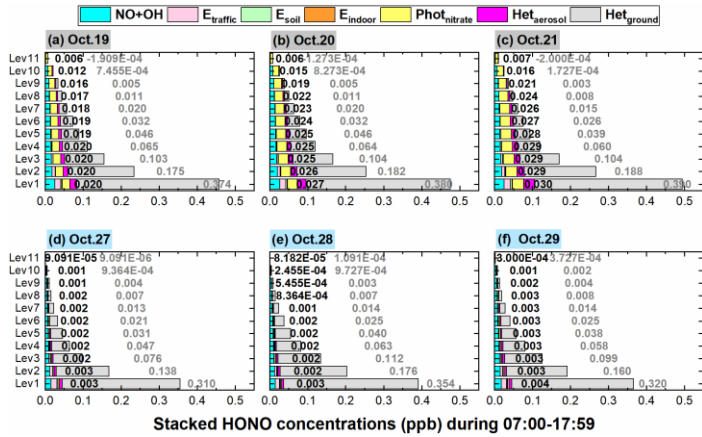
615 could be found in hazy days compared with clean days. In clean days the daytime
616 enhanced HONO by $\text{Phot}_{\text{nitrate}}$ was only 1–3 ppt in general and its contribution to
617 daytime HONO was usually <10%, while in the haze aggravating process, the
618 enhanced HONO concentration by $\text{Phot}_{\text{nitrate}}$ was about ten times higher than that in
619 clean days and $\text{Phot}_{\text{nitrate}}$ became the dominant HONO source (~30–70%) at higher
620 altitude, and both HONO concentrations and contributions by $\text{Phot}_{\text{nitrate}}$ increased with
621 the air pollution aggravation (**Fig.7a–c**, **Fig.8a–c**). The contributions of direct
622 emission sources were small and decreased when $\text{PM}_{2.5}$ increased, compared with
623 those heterogeneous reactions. Higher concentrations of NO_2 , nitrate, and $\text{PM}_{2.5}$
624 favored heterogeneous formation of HONO, while direct emission sources were
625 relatively invariable under different pollution levels.

626 Based on our results, nitrate concentrations increased with the haze aggravating
627 processes (**Fig.2b**), as a positive feedback effect, the elevated nitrate could in turn
628 enhance HONO formation and further enhance the atmospheric oxidation capacity
629 during daytime. Considering J_{nitrate} was still unclear, sensitivity tests were conducted
630 and are presented in the discussion section.

631

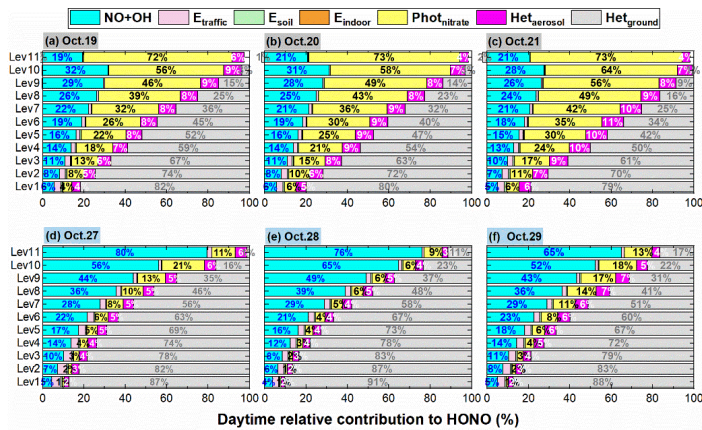
Deleted: one order of magnitude

Deleted: $\text{Phot}_{\text{nitrate}}$



634
 635 **Figure 7** The 95-NCP-site-averaged daytime HONO concentrations at different heights when the
 636 NO+OH reaction and the six potential HONO sources were included during a typical haze
 637 aggravating process of Oct.19–21 (a–c) and a clean period of Oct.27–29 (d–f) of 2018. (The first
 638 column numbers in black in each graph are for Phot_{nitrate}, and the second column numbers in gray
 639 are for Het_{ground}).

Deleted: .



641
 642 **Figure 8** The 95-NCP-site-averaged relative contributions of the NO+OH reaction and each of the
 643 six potential HONO sources to daytime HONO concentrations at different heights during a typical

645 haze aggravating process of Oct.19–21 (a–c) and a clean period of Oct.27–29 (d–f) of 2018. (The
646 first column numbers in blue in each graph are for the NO+OH reaction, the second column
647 numbers in black are for $\text{Phot}_{\text{nitrate}}$, the third column numbers in white are for $\text{Het}_{\text{aerosol}}$, and the
648 fourth column numbers in gray are for $\text{Het}_{\text{ground}}$).

649

650 3.3.2 Enhanced OH and its production rate

651 **Fig.9** demonstrates daytime variations of OH production (P(OH)) and loss
652 (L(OH)) rates near the surface and in the vertically-averaged layer (from ground to
653 the height of 2.5km) at the 95 NCP sites for the Base and 6S cases during Oct.11–31,
654 2018. A significant enhancement of P/L(OH) can be found near the surface and
655 vertically, the six potential HONO sources accelerated OH production and loss rates
656 remarkably near the surface and noticeably in the considered vertical layers.

657 Near the surface, daytime P(OH) and L(OH) were significantly enhanced by ~320%
658 for the 6S case (mean was 5.27 ppb h^{-1}) compared with the base case (mean was 1.26
659 ppb h^{-1}). For the base case, the daytime P(OH) via the photolysis of HONO and O_3
660 was 0.09 ppb h^{-1} and 0.09 ppb h^{-1} , respectively, while the daytime L(OH) via the
661 NO+OH reaction was 0.11 ppb h^{-1} and the net contribution of HONO photolysis to
662 P(OH) was -0.02 ppb h^{-1} . After adding the six potential HONO sources in case 6S, the
663 daytime P(OH) via the photolysis of HONO and O_3 was 1.81 ppb h^{-1} and 0.10 ppb h^{-1} ,
664 respectively, the daytime L(OH) via the NO+OH reaction was 0.48 ppb h^{-1} and the net
665 contribution of HONO photolysis to P(OH) reached 1.33 ppb h^{-1} . HONO photolysis

Deleted: .

Deleted: S

Deleted: could

Moved (insertion) [1]

Deleted: In short

Deleted: the

Deleted: photolysis

Deleted: photolysis

Deleted: .

Formatted: Superscript

Formatted: Superscript

674 was the main source of the primary formation of OH, while the secondary formed OH
 675 via [the reaction of HO₂+NO](#) (3.14 ppb h⁻¹) was the dominant source of the total OH
 676 formation.

Deleted:

677 Vertically, daytime P(OH) or L(OH) was enhanced by ~105% for the 6S case
 678 (mean was 2.21 ppb h⁻¹) compared with the base case (mean was 1.08 ppb h⁻¹). [For](#)
 679 [the base case, the daytime P\(OH\) via the photolysis of HONO and O₃ was 0.06 ppb](#)
 680 [h⁻¹ and 0.10 ppb h⁻¹, respectively, while the daytime L\(OH\) via the NO+OH reaction](#)
 681 [was 0.07 ppb h⁻¹ and the net contribution of HONO photolysis to P\(OH\) was -0.01](#)
 682 [ppb h⁻¹. After coupling the six potential HONO sources in case 6S, the daytime P\(OH\)](#)
 683 [via the photolysis of HONO and O₃ and via the HO₂+NO reaction was 0.48 ppb h⁻¹,](#)
 684 [0.12 ppb h⁻¹ and 1.52 ppb h⁻¹, respectively, the daytime L\(OH\) via the NO+OH](#)
 685 [reaction was 0.15 ppb h⁻¹ and the net contribution of HONO photolysis to P\(OH\) was](#)
 686 [0.33 ppb h⁻¹.](#)

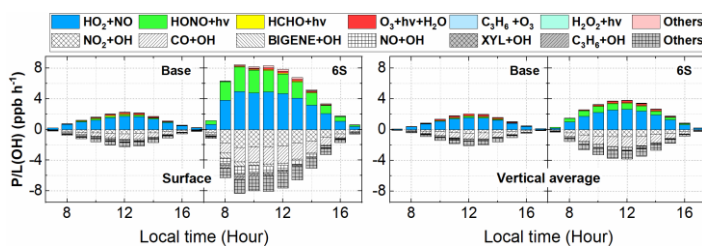
Deleted:),

Deleted: the

Deleted: photolysis

687

Moved up [1]: In short, the six potential HONO sources accelerated OH production and loss rates remarkably near the surface and noticeably in the considered vertical layers.



688

689 **Figure 9** Diurnal mean variations of OH production (P(OH)) and loss (L(OH)) rates including
 690 major production and loss reactions near the surface and in the vertically-averaged layer (from
 691 ground to the height of 2.5km) at the 95 NCP sites for the Base and 6S cases during Oct.11–31,
 692 2018.

700

701 **Fig.10** shows the linear relationships between daytime-averaged P(OH) and

702 PM_{2.5} concentrations and between daytime-averaged OH and PM_{2.5} concentrations

703 from ground to the height of 2.5km at the 95 NCP sites during Oct. 11–31 of 2018.

704 Both P(OH) for the two cases (Base and 6S) and the enhanced P(OH) due to the six

705 potential HONO sources showed a strong positive correlation ($r > 0.8$) with PM_{2.5}

706 concentrations at the 95 NCP sites, because Het_{aerosol}, Het_{ground} and Phot_{nitrate} were

707 significantly increased with the elevated PM_{2.5}. The enhanced P(OH) for the 6S case

708 reached 0.043 ppb h⁻¹ per 1 μg m⁻³ of a PM_{2.5} enhancement. Similarly, high positive

709 correlation ($r > 0.6$) could be found between OH and PM_{2.5} concentrations, the OH

710 concentrations and enhancements due to the six potential HONO sources were both

711 higher in hazy days than those in clean days, and the enhancement of OH reached

712 3.62×10^4 molec cm⁻³ per μg m⁻³ of PM_{2.5} for case 6S. These results were consistent

713 with a recent field study reported by Slater et al. (2020), who found that the OH

714 observed in haze events was elevated in central Beijing in November–December of

715 2016. Furthermore, two observations confirmed the key role of HONO in producing

716 primary OH despite the relatively lower photolysis frequency in haze aggravating

717 processes (Slater et al., 2020; Tan et al., 2018), consistent with our simulations

718 (**Fig.S7** shows the relationship between surface PM_{2.5} and photolysis frequencies of

719 NO₂, HONO and HNO₃ in this study).

Deleted: R

Formatted: Subscript

Formatted: Subscript

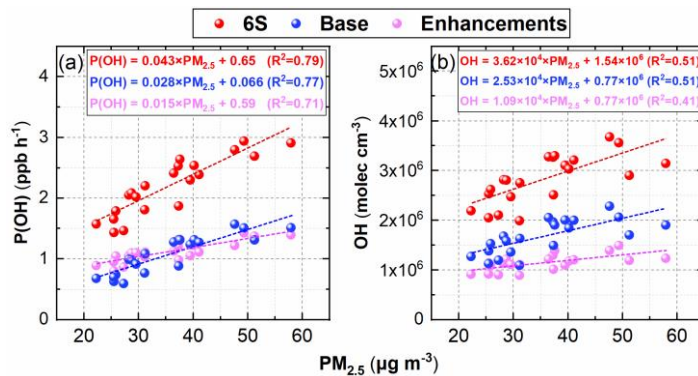
Deleted: , which are related to PM_{2.5} concentrations and solar radiation, are dominant potential HONO sources...

Deleted: and the

Formatted: Subscript

Deleted: R

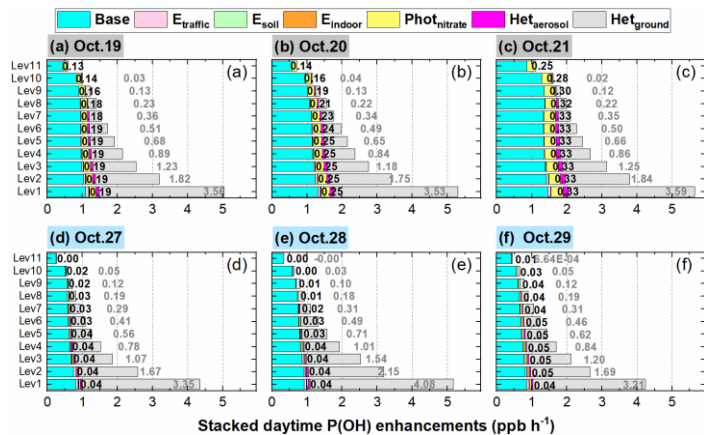
Deleted: S6



726
 727 **Figure 10** The linear relationships between daytime-averaged P(OH) and PM_{2.5} concentrations (a)
 728 and between daytime-averaged OH and PM_{2.5} concentrations (b) from ground to the height of
 729 2.5km at the 95 NCP sites during Oct. 11–31 of 2018.

730
 731 **Figs.11&12** show the detailed comparisons of P(OH) and OH enhancements
 732 during a haze aggravating process and a clean period. It can be seen that both P(OH)
 733 and OH were enhanced in hazy days compared with clean days, and P(OH) and OH
 734 increased with the aggravated haze pollution. Among the six potential HONO sources,
 735 Het_{ground} was the largest contributor to the enhanced P(OH) and OH near the surface,
 736 but its contribution was relatively stable under different pollution levels and was
 737 attenuated rapidly with height in both hazy and clean days; the contribution induced
 738 by Phot_{nitrate} was remarkably increased in haze aggravating processes and was about
 739 ten times higher than that in clean days; Het_{aerosol} also increased with the pollution
 740 levels but with relatively small values, while the impact of other three direct emission
 741 sources of HONO was quite small.

Deleted: one order of magnitude

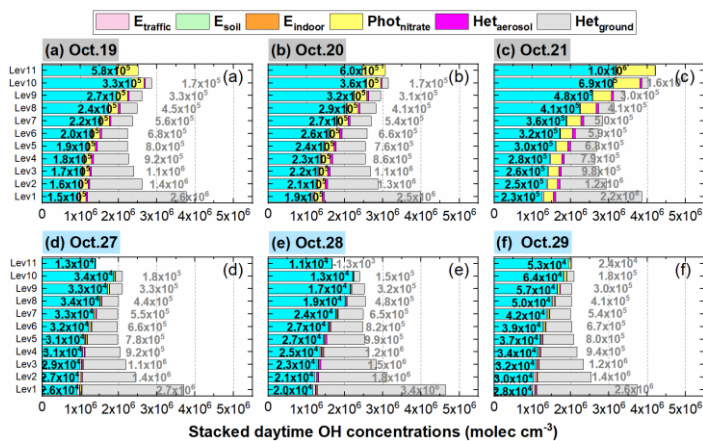


744

745 **Figure 11** The 95-NCP-site-averaged daytime P(OH) for the base case and the enhancements due to
 746 the six potential HONO sources during a typical haze aggravating process of Oct.19–21 (a–c)
 747 and a clean period of Oct.27–29 (d–f) of 2018. (The first column number in black in each graph is
 748 for Phot_{nitrate}, and the second column number in gray is for Het_{ground}).

749

Deleted: .



750

751 **Figure 12** The 95-NCP-site-averaged daytime OH concentrations for the base case and the
 752 enhancements due to the six potential HONO sources during a typical haze aggravating process of
 753 Oct.19–21 (a–c) and a clean period of Oct.27–29 (d–f) of 2018. (The first column number in black
 Deleted: .

Deleted: .

756 in each graph is for $\text{Phot}_{\text{nitrate}}$, and the second column number in gray is for $\text{Het}_{\text{ground}}$.

757

758 3.3.3 Enhanced DMA8 O₃

759 **Fig.13** demonstrates the linear relationship between DMA8 O₃ enhancements and

760 daytime PM_{2.5} concentrations in each vertical layer and the averaged vertical layer for

761 the considered eleven layers at the 95 NCP sites during Oct. 11–31 of 2018. A good

762 correlation ($r > 0.8$) between DMA8 O₃ enhancements and daytime PM_{2.5}

763 concentrations in the vertical averaged layer ([similar reasons for the strong positive](#)

764 [correlation between the enhanced P\(OH\) and PM_{2.5} concentrations shown above](#))

765 suggests that the enhanced O₃ due to the six potential HONO sources was larger in

766 polluted days and increased during the haze aggravating processes. The enhanced

767 DMA8 O₃ was < 2ppb when PM_{2.5} was < 20 $\mu\text{g m}^{-3}$ and was >10 ppb when PM_{2.5} was >

768 60 $\mu\text{g m}^{-3}$ on average, with a mean DMA8 O₃ enhancement of 0.24 ppb per $\mu\text{g m}^{-3}$ of

769 PM_{2.5}.

770

Deleted: 2

Deleted: (a)

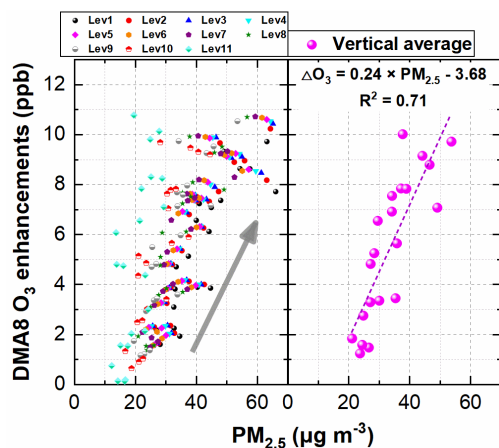
Deleted: (b)

Deleted:

Deleted: R

Deleted: ,

Deleted: u



778

779 **Figure 13** The linear relationship between DMA8 O₃ enhancements and daytime PM_{2.5}
 780 concentrations in each vertical layer (a) and the averaged vertical layer for the considered eleven
 781 layers (b) at the 95 NCP sites during Oct. 11–31 of 2018.

782

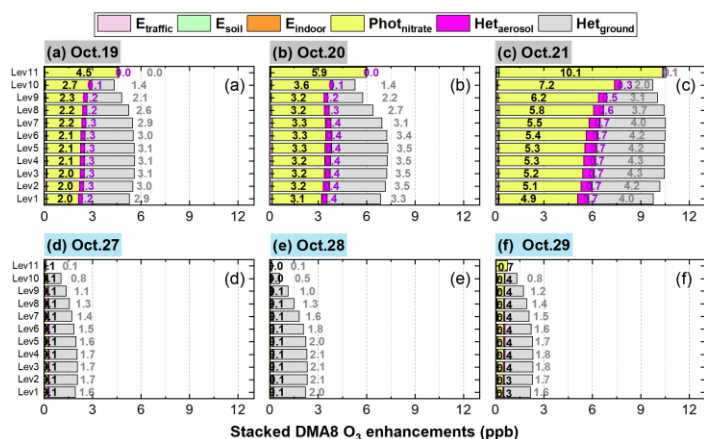
783 **Fig.14** shows the 95-NCP-site-averaged DMA8 O₃ enhancements due to the six
 784 potential HONO sources during a typical haze aggravating process of Oct.19–21 and
 785 a clean period of Oct.27–29 of 2018. A significant enhancement of DMA8 O₃ can be
 786 found during the haze aggravating process compared with during clean days. The
 787 enhanced DMA8 O₃ was ~5.5 ppb (Oct.19), ~ 7 ppb (Oct.20) and ~ 10 ppb (Oct.21),
 788 respectively, during the haze aggravating process, while that was usually ~2 ppb in
 789 clean days.

790 In clean days, Het_{ground} was the dominant contributor (~1.5–2 ppb) to the
 791 enhanced DMA8 O₃ among the six potential HONO sources, the contribution of
 792 Phot_{nitrate} to the enhanced DMA8 O₃ was ~0.1–0.4 ppb, while that of the other four
 793 sources was minor. When it comes to the comparison between the haze aggravating

794 process (Oct.19–21) and clean days, the DMA8 O₃ enhancements induced by Het_{ground}
 795 were doubled and reached ~3–4 ppb; the contribution of Phot_{nitrate} to the enhanced
 796 DMA8 O₃ substantially increased and reached ~2–4.5 ppb (Oct.19), ~3–6 ppb (Oct.20)
 797 and ~5–10 ppb (Oct.21), respectively; Het_{aerosol} showed an increasing contribution to
 798 the enhanced DMA8 O₃ during haze aggravating process (~0.3 ppb on Oct.19, ~0.4
 799 ppb on Oct.20 and ~0.7 ppb on Oct.21), while the impacts of the other three direct
 800 emission sources (E_{traffic}, E_{soil}, and E_{indoor}) on the enhanced DMA8 O₃ were minor.

Deleted: in
 Deleted: in
 Deleted: in

801



802

803 **Figure 14** The 95-NCP-site-averaged DMA8 O₃ enhancements due to the six potential HONO
 804 sources during a typical haze aggravating process of Oct.19–21 (a–c) and a clean period of
 805 Oct.27–29 (d–f) of 2018. (The column in black numbers in each graph is for Phot_{nitrate}, the column
 806 in purple numbers in each graph is for Het_{aerosol}, and the column in gray numbers is for Het_{ground}).

Deleted: .

807

812 3.4 Vertical variations of O₃-NO_x-VOCs sensitivity

813 Based on the results above, Phot_{nitrate} could significantly enhance the DMA8 O₃
814 by ten times in the considered vertical layers (especially at elevated heights) in
815 polluted events, but previous studies have not fully discussed. To better understand its
816 role in vertical O₃ formation, the O₃-NO_x-VOCs sensitivity was analyzed by using the
817 P(H₂O₂)/P(HNO₃) ratio proposed by Sillman (1995), which is more suitable than the
818 concentration ratio of H₂O₂/HNO₃ because of the large dry deposition velocity of the
819 two gases in the troposphere (Sillman, 1995). A transition point of P(H₂O₂)/P(HNO₃)
820 = 0.35 was suggested by Sillman (1995), when P(H₂O₂)/P(HNO₃) was <0.35, O₃
821 shows VOCs-sensitive chemistry (increasing VOC concentrations can significantly
822 elevate O₃ levels) and when P(H₂O₂)/P(HNO₃) was >0.35, O₃ tends to NO_x-sensitive
823 chemistry (increasing NO_x concentrations can significantly elevate O₃ levels).

824 **Fig.15** demonstrates the 95-NCP-site-averaged P(H₂O₂)/P(HNO₃) ratio at each
825 vertical layer for the 6S case during a typical haze aggravating process of Oct.19–21
826 and a clean period of Oct.27–29 of 2018. Obviously opposite O₃ sensitivity appeared
827 between the lower layers (VOCs sensitive) and the higher layers (NO_x sensitive) in
828 both clean and hazy days, and the transition point usually appeared at the eighth layer
829 (~600–800 m).

830 The Phot_{nitrate} reaction is assumed to produce HONO and NO_x (Zhou et al., 2003;
831 Romer et al., 2018; Gen et al., 2022), this reaction not only enhances OH
832 concentrations via HONO photolysis, but also directly releases NO_x back into the
833 troposphere. Considering the NO_x-sensitive O₃ chemistry at higher layers (>800m),

Deleted: one order of magnitude

Deleted: nitrate photolysis

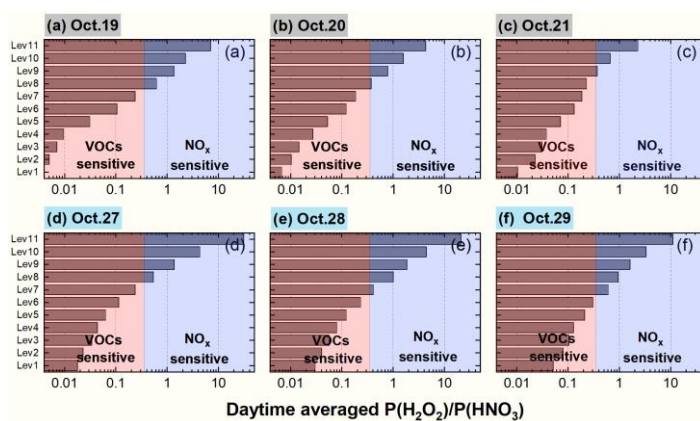
Formatted: Subscript

836 elevating OH and NO_x concentrations are both favorable for O₃ formation, especially
 837 in haze aggravating processes with abundant nitrate (detailed vertically enhanced O₃
 838 production/loss rates induced by Phot_{nitrate} are [shown in Fig.S8](#)).

Deleted: given

Deleted: 7

839



840

841 **Figure 15** The 95-NCP-site-averaged P(H₂O₂)/P(HNO₃) ratio at each vertical layer for the 6S case
 842 during a typical haze aggravating process of Oct.19–21 (a–c) and a clean period of Oct.27–29 (d–f)
 843 of 2018.

844

845 The specific role of the produced HONO or NO₂ via the [Phot_{nitrate}](#) reaction (R2) in
 846 DMA8 O₃ enhancements [was](#) further analyzed and is shown in **Fig. 16**, the produced

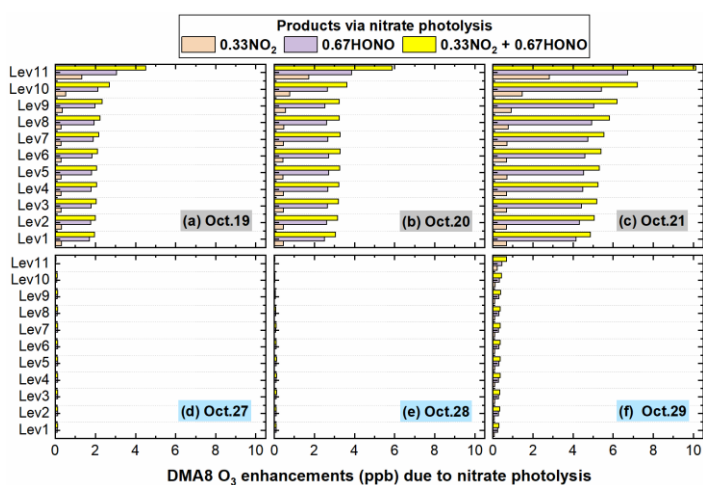
Deleted: nitrate photolysis

Formatted: Subscript

Deleted: were

847 NO₂ and HONO jointly promoted O₃ formation and increased DMA8 O₃
 848 concentrations. From the surface to ~1200m (Level 9), the DMA8 O₃ enhancements
 849 for case D_HONO was ~5 times those for case D_NO₂, while at ~2000 m (Level 11)
 850 the DMA8 O₃ enhancements for case D_HONO was ~2 times those for case D_NO₂.
 851 A balance exists between the propagation of the free radical interconversion cycle and
 852 the rate of termination of the cycle for the O₃ formation chemistry (Gligorovski et al.,

857 2015), considering the 0.67 and 0.33 yields (ratio is 2) for the two products, we could
 858 conclude that the impact of produced HONO on O₃ enhancements was larger than [that](#)
 859 [of](#) produced NO₂ near the surface, while at higher altitude (>2000 m) the impacts of
 860 the two products were similar.
 861



862
 863 **Figure 16** The 95-NCP-site-averaged DMA8 O₃ enhancements due to nitrate photolysis with three
 864 product scenarios (cases D_NO₂, D_HONO and D) during a typical haze aggravating process of
 865 Oct.19–21 (a–c) and a clean period of Oct.27–29 (d–f) in 2018.

867 **4. Discussion**

868 **4.1 Vertical variations of potential HONO sources**

869 The relative contribution of potential HONO sources near the surface,
 870 corresponding to the first model layer (0 to ~35 m) in our simulation, was quantified

871 in previous modelling studies (Fu et al., 2019; Xue et al., 2020; Zhang et al., 2021),
872 however, for those potential HONO sources, their relative contributions to HONO
873 concentrations near and above the surface should be different. Based on our results
874 **(Figs.7&8)**, the effects of aerosol related HONO sources would be severely
875 underestimated in hazy days when only focused surface HONO, especially for
876 $\text{Phot}_{\text{nitrate}}$. Near the surface in NCP, the daytime contribution of $\text{Phot}_{\text{nitrate}}$ to HONO
877 concentrations in hazy days was only ~4–6%, but this source contributed ~35–50% of
878 the enhanced DMA8 O₃ **(Fig.14a–c)**; above the eighth layer (~800 m), this source
879 contributed ~50–70% of HONO concentrations and ~50–95% of the enhanced DMA8
880 O₃ **(Fig.14a–c)**.

881 A recent observation in urban Beijing reported vertical HONO concentrations
882 from three heights above the ground and found that extremely high HONO
883 concentrations occurred at 120 m (~5 ppb) and 240 m (~3 ppb) rather than near the
884 surface (~1.2 ppb) during 12:00 in a typical hazy day (Zhang et al., 2020b). The
885 observation was unusual at noontime under strong convection conditions, inconsistent
886 with those most previous observations indicating a HONO decrease trend with height,
887 especially with the observational results of Zhu et al. (2011) and Meng et al. (2020)
888 and simulated results of Zhang et al. (2021) **and ours in Fig.S6** at the same
889 observational site. The contributions of different HONO sources at each layer were
890 analyzed by using a box model, but ~80–90% of the noontime HONO at higher layers
891 could not be explained by the known HONO formation mechanisms (Zhang et al.,
892 2019c). The box model neglected the vertical convection, so the ground related

Formatted: Font: Bold

Deleted: nitrate photolysis

Formatted: Subscript

Deleted: surface

Formatted: Font: Bold

Deleted: (including our simulations in Fig.S5)

896 HONO sources had no contribution to HONO concentrations at the higher layers, thus
897 their HONO simulations were actually underestimated compared with our results and
898 the previous studies of Wong et al. (2011) and Zhang et al. (2021).

899

900 4.2 Uncertainties of $J_{\text{nitrate}}/J_{\text{HNO}_3}$ ratios and their impacts

901 4.2.1 Uncertainties of $J_{\text{nitrate}}/J_{\text{HNO}_3}$ ratios in DMA8 O₃ enhancements

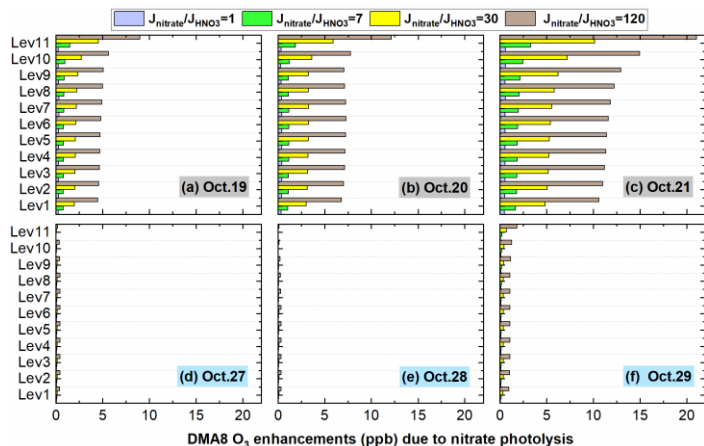
902 Based on our results, $\text{Het}_{\text{ground}}$ and $\text{Phot}_{\text{nitrate}}$ were the two major contributors to
903 the enhanced DMA8 O₃, especially for $\text{Phot}_{\text{nitrate}}$ in hazy days with higher PM_{2.5}
904 concentrations. The uncertainties of $\text{Phot}_{\text{nitrate}}$ (four $J_{\text{nitrate}}/J_{\text{HNO}_3}$ ratios) in O₃
905 enhancements were analyzed and are shown in Fig.17 (The uncertainties of $\text{Het}_{\text{ground}}$
906 are presented in text S2). During the haze aggravating process, the enhanced DMA8
907 O₃ near the surface increased from ~0.3 to ~0.5 ppb, from ~0.9 to ~2 ppb, from ~2 to
908 ~6 ppb, and from ~5 to ~12 ppb, with the $J_{\text{nitrate}}/J_{\text{HNO}_3}$ ratio being 1, 7, 30, 120,
909 respectively, and the enhanced O₃ increased with altitude. In clean days, the impact of
910 $\text{Phot}_{\text{nitrate}}$ on O₃ enhancements was small (<1 ppb) even with a $J_{\text{nitrate}}/J_{\text{HNO}_3}$ ratio of
911 120.

912

Deleted: the

Deleted: for

Deleted: given



916
 917 **Figure 17** The 95-NCP-site-averaged DMA8 O₃ enhancement induced by nitrate photolysis with
 918 four $J_{\text{nitrate}}/J_{\text{HNO}_3}$ ratios (1, 7, 30 and 120) during a typical haze aggravating process of Oct.19–21
 919 (a–c) and a clean period of Oct.27–29 (d–f) of 2018.

920

921 4.2.2 Uncertainties of $J_{\text{nitrate}}/J_{\text{HNO}_3}$ ratios in nitrate concentrations

922 We found considerable enhancements in O₃ concentrations induced by $\text{Phot}_{\text{nitrate}}$,
 923 yet it is still unclear that to what extent $\text{Phot}_{\text{nitrate}}$ could influence nitrate
 924 concentrations. The overall nitrate concentrations for the base case and the nitrate
 925 enhancements induced by the potential HONO sources decreased with rising altitude
 926 except for $\text{Phot}_{\text{nitrate}}$ (Fig.S9a). $\text{Het}_{\text{ground}}$ enhanced nitrate concentrations by $\sim 1.5 \mu\text{g}$
 927 m^{-3} near the surface and the enhancements decreased to $< 0.5 \mu\text{g} \text{m}^{-3}$ above the eighth
 928 model layer ($\sim 800\text{m}$); the nitrate enhancements due to $\text{Het}_{\text{aerosol}}$ and E_{traffic} near the
 929 surface were ~ 0.2 and $\sim 0.1 \mu\text{g} \text{m}^{-3}$, respectively, and were < 0.1 and $< 0.04 \mu\text{g} \text{m}^{-3}$
 930 above the sixth model layer ($\sim 500\text{m}$). For $\text{Phot}_{\text{nitrate}}$, the overall impact of four

Deleted: nitrate photolysis
 Formatted: Subscript
 Deleted: nitrate photolysis
 Formatted: Subscript

Deleted: S8a

934 $J_{\text{nitrate}}/J_{\text{HNO}_3}$ ratios on nitrate concentrations is shown in **Fig.S9b**, a smaller $J_{\text{nitrate}}/J_{\text{HNO}_3}$
935 ratio of 1 or 7 had a limited impact on nitrate concentrations of $\sim 0\text{--}0.05 \mu\text{g m}^{-3}$, a
936 $J_{\text{nitrate}}/J_{\text{HNO}_3}$ ratio of 30 slightly decreased nitrate concentrations by $\sim 0.2 \mu\text{g m}^{-3}$, while
937 the $J_{\text{nitrate}}/J_{\text{HNO}_3}$ ratio of 120 decreased vertical nitrate concentrations by $\sim 0.3\text{--}0.8 \mu\text{g}$
938 m^{-3} . The relative nitrate changes caused by $\text{Phot}_{\text{nitrate}}$ were calculated by the
939 differences between four cases added $\text{Phot}_{\text{nitrate}}$ (cases Nit_1, Nit_7, D and Nit_120)
940 and the base case (**Fig.S9c**). The vertical nitrate concentrations were reduced by $\sim 0\text{--}$
941 0.4% ($J_{\text{nitrate}}/J_{\text{HNO}_3}=1$), $\sim 0\text{--}2\%$ (7), $\sim 2\text{--}5\%$ (30) and $\sim 10\text{--}14\%$ (120) at the 95 NCP
942 sites, meaning that the $\text{Phot}_{\text{nitrate}}$ impact on vertical nitrate concentrations is limited
943 ($<5\%$) when adopting a relatively small $J_{\text{nitrate}}/J_{\text{HNO}_3}$ ratio (< 30) (**Fig.S9c**).

944 **Romer et al. (2018) found a $J_{\text{nitrate}}/J_{\text{HNO}_3}$ ratio of 10 or 30 had a much larger effect**
945 **on HONO than on HNO_3 , and $\text{Phot}_{\text{nitrate}}$ accounted for an average of 40% of the total**
946 **production of HONO, and only 10% of HNO_3 loss with a $J_{\text{nitrate}}/J_{\text{HNO}_3}$ ratio of 10**
947 **(Fig.5 in Romer et al. (2018)), consistent with our study. From the production rate of**
948 **gas HNO_3 (P_{HNO_3}) in Fig.S10, we can find that an increase in the $J_{\text{nitrate}}/J_{\text{HNO}_3}$ ratio for**
949 **$\text{Phot}_{\text{nitrate}}$ simultaneously enhances the HNO_3 production rate, and is favorable for**
950 **nitrate formation via the reaction between HNO_3 and NH_3 . Nitrate consumption is**
951 **mitigated by the faster nitrate formation, this is the main reason for less perturbation**
952 **of the nitrate budget influenced by $\text{Phot}_{\text{nitrate}}$.**

953 **Fig.18 shows the detailed relative changes of nitrate caused by $\text{Phot}_{\text{nitrate}}$ during a**
954 **typical haze aggravating process and a clean period (corresponding concentrations are**
955 **shown in Fig.S11). The percentage nitrate reduction was usually smaller in hazy days**

Deleted: S8b

Deleted: ,

Deleted: the

Deleted: S8c

Formatted: Subscript

Formatted: Subscript

Formatted: Subscript

Formatted: Subscript

Deleted: HONO

Deleted: but

Formatted: Subscript

Formatted: Subscript

Formatted: Subscript

Deleted: which is

Deleted: gaseous HNO_3

Formatted: Subscript

Formatted: Subscript

Formatted: Font: Bold

Deleted: could

Deleted: increasing

Formatted: Subscript

Formatted: Subscript

Formatted: Subscript

Deleted: cing

Formatted: Subscript

Deleted: which

Formatted: Subscript

Formatted: Subscript

Deleted: was

Deleted: why

Formatted: Subscript

Deleted: nitrate

Deleted: were

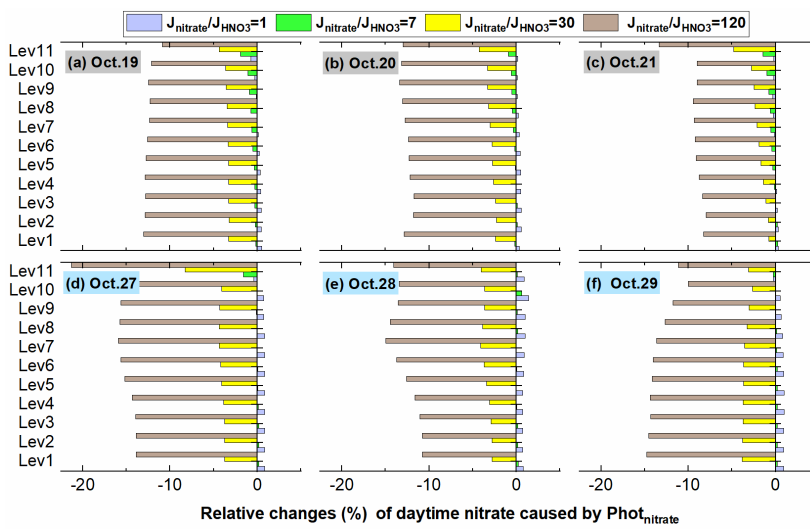
Deleted: S9

Deleted:),

Deleted: the

975 than in clean days, mainly due to the slightly weaker photolysis frequency in pollution
 976 events (Fig.S7). The nitrate reduction was <5% when adopting a $J_{\text{nitrate}}/J_{\text{HNO}_3}$ ratio of
 977 30 in both clean and hazy days and was <15% in most cases even when the
 978 $J_{\text{nitrate}}/J_{\text{HNO}_3}$ ratio reached 120.

979



980

981 **Figure 18** The 95-NCP-site-averaged relative changes of nitrate with four $J_{\text{nitrate}}/J_{\text{HNO}_3}$ ratios (1, 7,
 982 30 and 120) compared with the base case, during a typical haze aggravating process of Oct.19–21
 983 (a–c) and a clean period of Oct.27–29 (d–f) of 2018.

984

985 4.2.3 Possible ranges of the $J_{\text{nitrate}}/J_{\text{HNO}_3}$ ratio

986 From the above discussion, we can find that the enhanced OH and O₃ due to
 987 Phot_{nitrate} are remarkable during haze aggravating processes, and the exact value of the
 988 $J_{\text{nitrate}}/J_{\text{HNO}_3}$ ratio requires more studies.

- Formatted: Font: Bold
- Deleted: and nitrate was slightly reduced during the haze aggravating processes, t...
- Deleted: the
- Deleted: in
- Deleted: days
- Deleted: of the
- Deleted: .

- Deleted: nitrate
- Deleted: (c)

998 **Fig. 19** shows diurnal patterns of surface-averaged and vertically-averaged
999 simulations of the $J_{\text{Phot}_{\text{nitrate}}}$ frequency with four different $J_{\text{nitrate}}/J_{\text{HNO}_3}$ ratios at the 95
1000 NCP sites during the study period. The $J_{\text{Phot}_{\text{nitrate}}}$ frequency at 12:00 was 3.7×10^{-7} ,
1001 2.6×10^{-6} , 1.1×10^{-5} and $4.5 \times 10^{-5} \text{ s}^{-1}$, when adopting a $J_{\text{nitrate}}/J_{\text{HNO}_3}$ ratio of 1, 7, 30 and
1002 120, respectively. The corresponding vertically-averaged $J_{\text{Phot}_{\text{nitrate}}}$ frequency was
1003 slightly larger ($\sim 10\%$) and was 4.2×10^{-7} , 2.9×10^{-6} , 1.3×10^{-5} and $5.0 \times 10^{-5} \text{ s}^{-1}$,
1004 respectively. Adopting a $J_{\text{nitrate}}/J_{\text{HNO}_3}$ ratio of 30 in the 6S case, with the corresponding
1005 J_{nitrate} of $1.1\text{--}1.3 \times 10^{-5} \text{ s}^{-1}$, produced $\sim 30\text{--}50\%$ of the enhanced O_3 near the surface in
1006 hazy days (**Fig.13**), and $\sim 70\text{--}90\%$ of the enhanced O_3 at higher layers ($>800 \text{ m}$).

1007 The reported values of J_{nitrate} from previous studies are summarized in **Table 4**.
1008 The experimental J_{nitrate} values have been controversial over the past two decades and
1009 are still arguable currently. In our simulations for the 6S case, $J_{\text{Phot}_{\text{nitrate}}}$ contributed
1010 from $\sim 1\%$ (clean days) to $\sim 5\%$ (hazy days) to surface HONO during daytime when
1011 using the $J_{\text{nitrate}}/J_{\text{HNO}_3}$ ratio of 30 in NCP, consistent with $<8\%$ at a rural site in NCP
1012 reported by Xue et al. (2020) and $\sim 1\%$ at urban Beijing reported by Zhang et al. (2021)
1013 using the same ratio; however, the increasing contribution of $J_{\text{Phot}_{\text{nitrate}}}$ to HONO
1014 concentrations with rising altitude based on our simulations (**Fig.7**), has not been
1015 discussed in previous research. Furthermore, we found that the overall $J_{\text{Phot}_{\text{nitrate}}}$
1016 impact to OH and O_3 would be severely underestimated when the $J_{\text{Phot}_{\text{nitrate}}}$
1017 contribution to vertical HONO was excluded.

1018 A larger $J_{\text{nitrate}}/J_{\text{HNO}_3}$ ratio of 120 for $J_{\text{Phot}_{\text{nitrate}}}$ ($4.5\text{--}5.0 \times 10^{-5} \text{ s}^{-1}$ at 12:00) produced
1019 $\sim 25\text{--}30\%$ of noontime HONO in NCP in our study (**Fig.S12**), comparable with $30\text{--}40\%$

Deleted: nitrate photolysis

Formatted: Subscript

Deleted: nitrate photolysis

Formatted: Subscript

Deleted: nitrate photolysis

Formatted: Subscript

Deleted: nitrate photolysis

Formatted: Subscript

Deleted: nitrate photolysis

Formatted: Subscript

Formatted: Subscript

Deleted: of nitrate photolysis

Formatted: Subscript

Deleted: of nitrate photolysis

Deleted: nitrate photolysis

Formatted: Subscript

Deleted: S10

1029 in previous modelling studies (Fu et al., 2019; Shi et al., 2020) when using the
1030 $J_{\text{nitrate}}/J_{\text{HNO}_3}$ ratio of 118.57 ($8.3 \times 10^{-5}/ 7 \times 10^{-7}$). In haze aggravating processes, the
1031 contribution of $\text{Phot}_{\text{nitrate}}$ ($J_{\text{nitrate}}/J_{\text{HNO}_3} = 120$) to the DMA8 O_3 enhancements reached
1032 $\sim 5\text{--}10$ ppb near the surface and $\sim 8\text{--}20$ ppb above the tenth model layer (**Fig.17**), these
1033 enhancements were extremely large. In a previous modelling study by Fu et al. (2020),
1034 the daytime surface O_3 simulations were systematically overestimated by ~ 5 ppb in
1035 NCP in winter (**Fig.S4** in Fu et al. (2020)), the inclusion of $\text{Phot}_{\text{nitrate}}$ ($J_{\text{nitrate}}/J_{\text{HNO}_3} =$
1036 118.57) in their study might cause the overestimation. From the above, a $J_{\text{nitrate}}/J_{\text{HNO}_3}$
1037 ratio of 120, or a J_{nitrate} value of $\sim 4\text{--}5 \times 10^{-5} \text{ s}^{-1}$ is possibly overestimated. When
1038 adopting the maximum J_{nitrate} value of 10^{-4} s^{-1} reported by Ye et al. (2016a) and Bao et
1039 al. (2018), we reasonably speculate that O_3 simulations will be significantly
1040 overestimated, especially at higher altitude with NO_x -sensitive O_3 chemistry (**Fig.15**).

1041 Romer et al. (2018) and Kasibhatla et al. (2018) suggested that a $J_{\text{nitrate}}/J_{\text{HNO}_3}$ ratio
1042 of 30 or smaller would be more suitable, being about the minimum value reported by
1043 Ye et al. (2016a) and Bao et al. (2018), this ratio has shown significant influence on
1044 the O_3 simulations in haze aggravating processes in this study. The lack of
1045 photo-catalyzer in suspended submicron particulate sodium and ammonium nitrate
1046 may cause a lower $J_{\text{nitrate}}/J_{\text{HNO}_3}$ ratio (<10) reported by Shi et al. (2021), so more
1047 chamber experiments need to be conducted by using the particles collected in the real
1048 atmosphere. Choosing a larger J_{nitrate} value might cover up other ground-based
1049 unknown HONO sources, creating an illusion of good model simulations of daytime
1050 HONO, but resulting in overestimation of O_3 concentrations. Considering the

Deleted: s

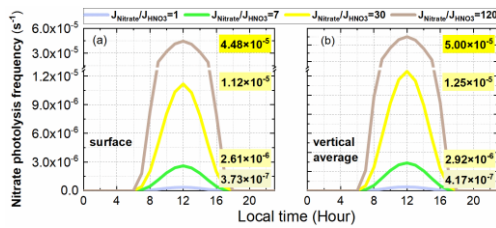
Deleted: and

Deleted: ly

Deleted: d

Deleted: to

1056 uncertainties of NO_x or VOCs emissions, which also significantly impact O₃
 1057 simulations, more studies are needed to find the exact value of J_{nitrate} in the real
 1058 atmosphere.
 1059



1060
 1061 **Figure 19** Diurnal patterns of surface-averaged (a) and vertically-averaged (b) simulations of the
 1062 nitrate photolysis frequency with four different J_{nitrate}/J_{HNO₃} ratios (1, 7, 30, 120) at the 95 NCP
 1063 sites during the study period (The nitrate photolysis frequencies at 12:00 are shown in each graph).

Deleted: is

1064
 1065
 1066
 1067 **Table 4.** Summary of studies on the nitrate photolysis frequency (J_{nitrate}) (J_{HNO₃} denotes the photolysis
 1068 frequency of gas HNO₃)

Experimental conditions	Main conclusion	Reference
HNO ₃ absorbed on Pyrex surface	J _{nitrate} (1.2×10 ⁻⁵ s ⁻¹) is 1–2 orders of magnitude faster than in the gas and aqueous phases.	(Zhou et al., 2003)
Atmosphere simulation chamber	J _{nitrate} on snow, ground, and glass surfaces, can be excluded in the chamber.	(Rohrer et al., 2005)
HNO ₃ absorbed on glass surface	Photolysis frequency of surfaces adsorbed HNO ₃ is > 2 orders of magnitude larger than J _{HNO₃} .	(Zhu et al., 2008)
Urban grime-coated surface	J _{nitrate} (1.2×10 ⁻³ s ⁻¹) is 4 orders of magnitude faster than in water (10 ⁻⁷ s ⁻¹).	(Baergen and Donaldson, 2013)
Various natural/artificial surfaces	J _{nitrate} ranges from 6.0×10 ⁻⁶ s ⁻¹ to 3.7×10 ⁻⁴ s ⁻¹ , 1–3 orders of magnitude higher than J _{HNO₃}	(Ye et al., 2016a)
Adsorbed HNO ₃ on glass surfaces	Photolysis frequency of surfaces adsorbed HNO ₃ (2.4×10 ⁻⁷ s ⁻¹) is very low.	(Laufs and Kleffmann, 2016)

Aerosol filter samples	J_{nitrate} ranges from $6.2 \times 10^{-6} \text{ s}^{-1}$ to $5.0 \times 10^{-4} \text{ s}^{-1}$ with a mean of $1.3 \times 10^{-4} \text{ s}^{-1}$.	(Ye et al., 2017)
Nitrate aerosol in the MBL	J_{nitrate} is ~ 10 times higher than J_{HNO_3} .	(Reed et al., 2017)
PM _{2.5} in Beijing	J_{nitrate} ($1.22 \times 10^{-5} \text{ s}^{-1}$ to $4.84 \times 10^{-4} \text{ s}^{-1}$) is 1–3 orders of magnitude higher than J_{HNO_3} .	(Bao et al., 2018)
Sea-salt particulate nitrate	J_{nitrate} is 25–50 times higher than J_{HNO_3} .	(Kasibhatla et al., 2018)
Particles collected on filters	J_{nitrate} is ≤ 30 times J_{HNO_3} .	(Romer et al., 2018)
CMAQ simulation	Nitrate photolysis contributed $\sim 30\%$ of noontime HONO with a $J_{\text{nitrate}}/J_{\text{HNO}_3}$ ratio of ~ 120 .	(Fu et al., 2019)
CMAQ simulation	A $J_{\text{nitrate}}/J_{\text{HNO}_3}$ ratio of 100 better improved sulfate simulations than a $J_{\text{nitrate}}/J_{\text{HNO}_3}$ ratio of 10.	(Zheng et al., 2020)
MCM Box model	Nitrate photolysis contribution to HONO was $< 8\%$ with a $J_{\text{nitrate}}/J_{\text{HNO}_3}$ ratio of 30.	(Xue et al., 2020)
MCM Box model	Nitrate photolysis contributed $\sim 40\%$ of noontime HONO with a $J_{\text{nitrate}}/J_{\text{HNO}_3}$ ratio of ~ 120 .	(Shi et al., 2020)
Smog chamber	The $J_{\text{nitrate}}/J_{\text{HNO}_3}$ ratio was < 10 for suspended submicron NaNO_3 and NH_4NO_3 .	(Shi et al., 2021)
CMAQ simulation	Nitrate photolysis contribution to surface HONO was $\sim 1.0\%$ with a $J_{\text{nitrate}}/J_{\text{HNO}_3}$ ratio of 30.	(Zhang et al., 2021)
WRF-Chem simulation	The relative contribution of nitrate photolysis to HONO increased with rising altitude and nitrate photolysis contributed much larger in the ABL than near the surface to the enhanced O_3 . On average, nitrate photolysis contributed $\sim 5\%$ of surface daytime HONO with a $J_{\text{nitrate}}/J_{\text{HNO}_3}$ ratio of 30 ($\sim 1 \times 10^{-5} \text{ s}^{-1}$) but contributed $\sim 30\text{--}50\%$ of the enhanced O_3 near the surface in NCP in hazy days.	This study

Deleted: the enhanced O_3
Deleted: HONO
Formatted: Subscript

1070 MBL: marine boundary layer; ABL: atmospheric boundary layer.

Formatted: Line spacing: Double

1071

Deleted: 4

1072

Deleted: The i

1073

Deleted: the

Formatted: Font color: Text 1

1074 **4.3 Interactions between heterogeneous HONO sources**

Formatted: Line spacing: Double

Formatted: Font: Bold, Font color: Text 1

Formatted: Font color: Text 1

1075 Form the comparison of nitrate budget induced by the six potential HONO

Deleted: cloud clearly

Deleted: the nitrate concentrations were increased by

1076 sources in Fig.S3&S9, we can find that $\text{Het}_{\text{ground}}$ led to an significant increase in

Formatted: Font color: Text 1, Subscript

Formatted: Font color: Text 1

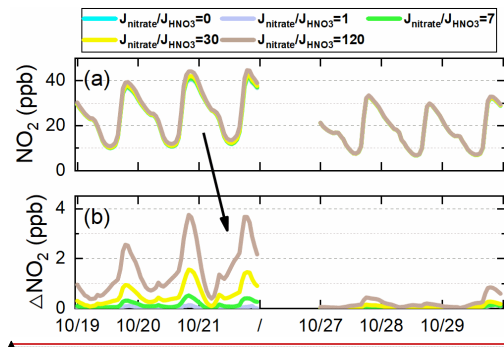
1077 nitrate concentrations. In the real atmosphere, the NO_2 heterogeneous reactions and

Formatted: Font color: Text 1, Subscript

Formatted: Font color: Text 1

1085 the J_{nitrate} reaction occur simultaneously, while the sensitivity tests only considered
 1086 one specific HONO source for each case and neglected their interactions, leading to
 1087 the underestimation of the J_{nitrate} impact to some extent. Take it into consideration,
 1088 the J_{nitrate} impact on atmospheric oxidants and secondary pollutants would be even
 1089 larger, especially during the haze aggravating process.

1090 J_{nitrate} would in turn change NO_x concentrations to some extent. From the
 1091 95-site-averaged NO_2 concentrations shown in Fig. 20, we can find that J_{nitrate}
 1092 slightly increased NO_2 concentrations in hazy days. The elevated NO_2 concentration
 1093 could enhance HONO formation via the NO_2 heterogeneous reactions, nevertheless,
 1094 due to the high background NO_2 concentrations in NCP (up to ~ 40 ppb at nighttime),
 1095 the increment of NO_2 and the enhanced HONO formation from NO_2 caused by
 1096 J_{nitrate} were small (<10%), but might have a larger impact on NO_x budgets in clean
 1097 regions. From the above, a positive feedback relationship between the NO_2
 1098 heterogeneous reactions and the J_{nitrate} reaction could be found, these
 1099 multi-processes worse the air quality during the haze aggravating processes.



1100

Deleted: nitrate photolysis

Formatted

Deleted: s were occurred ...ccur simultaneously, while the

Formatted

Deleted: impact of

Deleted: The nitrate photolysis

Formatted: Font: Not Italic, Font color: Text 1

Formatted: Indent: First line: 0.74 cm, Line spacing: Double

Formatted

Deleted: s

Deleted: find that nitrate photolysis

Formatted

Deleted: below

Formatted

Deleted: could

Formatted: Font color: Text 1

Formatted

Deleted: e

Formatted

Deleted: nitrate photolysis

Formatted

Deleted: was

Formatted

Deleted: this process

Formatted

Deleted: to

Formatted

Deleted: nitrate photolysis

Formatted

Deleted: s

Formatted: Font: Not Italic, Font color: Text 1

Formatted: Font color: Text 1

Formatted: Font color: Text 1

1138 **Figure 20** Comparison of 95-site-averaged simulations of NO₂ concentrations for the base case and
1139 four cases with different J_{nitrate}/J_{HNO₃} ratios (1, 7, 30 and 120) (a), and the corresponding NO₂ variations
1140 (b) compared with the base case in the North China Plain during Oct.11–31 of 2018.

- Deleted: 1
- Deleted: mean
- Deleted: simulated
- Deleted: the
- Deleted: added Phot_{nitrate}
- Deleted: hourly

1141

1148 **5. Conclusions**

1149 In this study, three direct emission sources, the improved NO₂ heterogeneous
1150 reactions on aerosol and ground surfaces, and particulate nitrate photolysis in the
1151 atmosphere were included into the WRF-Chem [model](#) to explore the key [HONO](#)
1152 sources producing O₃ enhancements during typical autumn haze aggravating
1153 processes with co-occurrence of high PM_{2.5} and O₃ in NCP. The six potential HONO
1154 sources produced a significant enhancement in surface HONO simulations and
1155 improved the mean HONO concentration at the BUCT site to 1.47 ppb from 0.05 ppb
1156 (improved the NMB to -14.22% from -97.11% and the IOA to 0.80 from 0.45). The
1157 improved HONO significantly enhanced the atmospheric oxidation capacity near the
1158 surface and at elevated heights, especially in hazy days, resulting in fast formation of
1159 and significant improvements of O₃ during haze aggravating processes in NCP.
1160 Although the photolysis frequency is usually lower during hazy days, higher
1161 concentrations of NO₂, PM_{2.5} and nitrate favored HONO formation via heterogeneous
1162 reactions, leading to stronger atmospheric oxidation capacity. The major results
1163 include:

1164 (1) For the surface HONO in NCP, Het_{ground} was the largest source during
1165 daytime and nighttime (~50–80%); the contribution of Phot_{nitrate} ($J_{\text{nitrate}}/J_{\text{HNO}_3} = 30$) to
1166 surface HONO concentrations was close to that of the NO+OH reaction during
1167 daytime (~1–12%) and was ~5% for daytime average; E_{traffic} was important during
1168 nighttime (~10–20%) but small during daytime (<5%); the contribution of Het_{aerosol}
1169 was minor (~2–3%) in daytime and <10% in nighttime; the contribution of E_{soil} was

Deleted: of HONO

Deleted: 86

Deleted: 78

1173 <3%, and E_{indoor} could be neglected. Vertically, the HONO enhancements due to
1174 ground-based potential HONO sources (E_{traffic} , E_{soil} , E_{indoor} and H_{etground}) decreased
1175 rapidly with height, while the NO+OH reaction and aerosol-related HONO sources
1176 ($Phot_{\text{nitrate}}$ and $H_{\text{et aerosol}}$) decreased with height much slower. The enhanced HONO
1177 due to $Phot_{\text{nitrate}}$ in hazy days was about ten times larger than in clean days and
1178 became the dominant HONO source (~30–70% when $J_{\text{nitrate}}/J_{\text{HNO}_3} = 30$) at higher
1179 layers, and both HONO concentrations and $Phot_{\text{nitrate}}$ contributions increased with the
1180 aggravated pollution levels.

Deleted: one order of magnitude

1181 (2) Near the surface, daytime OH production/loss rates were significantly
1182 enhanced by ~320% for the 6S case (mean was 5.27 ppb h^{-1}) compared with the base
1183 case (mean was 1.26 ppb h^{-1}); vertically, daytime OH production/loss rates were
1184 enhanced by ~105% for the 6S case (mean was 2.21 ppb h^{-1}) compared with the base
1185 case (mean was 1.08 ppb h^{-1}). The enhanced OH production rate and OH due to the
1186 six potential HONO sources both showed a strong positive correlation with $PM_{2.5}$
1187 concentrations at the 95 NCP sites, with a slope of $0.043 \text{ ppb h}^{-1}/\mu\text{g m}^{-3}$ of $PM_{2.5}$ and
1188 $3.62 \times 10^4 \text{ molec cm}^{-3}/\mu\text{g m}^{-3}$ of $PM_{2.5}$ from the surface to the height of 2.5 km for case
1189 6S, respectively. The atmospheric oxidation capacity (e.g., OH) was enhanced in the
1190 haze aggravating process.

1191 (3) A strong positive correlation ($r > 0.8$) between enhanced O_3 by the six potential
1192 HONO sources and $PM_{2.5}$ concentrations was found in NCP, and nitrate photolysis
1193 was the largest contributor to the enhanced DMA8 O_3 in hazy days. Vertically, the
1194 enhanced DMA8 O_3 was < 2ppb when $PM_{2.5}$ was < $20 \mu\text{g m}^{-3}$, and that was >10 ppb

1196 when $PM_{2.5}$ was $> 60\mu\text{g m}^{-3}$ on average, with a slope of 0.24 ppb DMA8 O_3
1197 enhancement $/\mu\text{g m}^{-3}$ of $PM_{2.5}$. The surface enhanced DMA8 O_3 was ~ 5.5 ppb
1198 (Oct.19), ~ 7 ppb (Oct.20) and ~ 10 ppb (Oct.21), respectively, during a typical haze
1199 aggravating process, while that was usually ~ 2 ppb in clean days. The contribution of
1200 $Phot_{\text{nitrate}}$ to the enhanced DMA8 O_3 was increased by over one magnitude during the
1201 haze aggravating process (up to 5–10 ppb) compared with that in clean days (~ 0.1 – 0.5
1202 ppb), reached ~ 2 – 4.5 ppb (Oct.19), ~ 3 – 6 ppb (Oct.20) and ~ 5 – 10 ppb (Oct.21),
1203 respectively, during a typical haze aggravating process vertically.

Deleted: and

1204 (4) Surface O_3 was controlled by VOCs-sensitive chemistry, while O_3 at higher
1205 altitude ($>800\text{m}$) was controlled by NO_x -sensitive chemistry in NCP during autumn.
1206 The nitrate photolysis reaction enhanced OH and NO_x concentrations, both favored O_3
1207 formation at high altitude, especially in haze aggravating processes with abundant
1208 nitrate. The produced HONO rather than the produced NO_2 through nitrate photolysis
1209 had a stronger promotion for O_3 formation near the surface, but the impacts of the two
1210 products on O_3 enhancements were similar at higher altitude (~ 2000 m).

1211 (5) Nitrate photolysis only contributed $\sim 5\%$ of the surface HONO in daytime
1212 with a $J_{\text{nitrate}}/J_{\text{HNO}_3}$ ratio of 30 ($\sim 1 \times 10^{-5} \text{ s}^{-1}$) but contributed ~ 30 – 50% of the enhanced
1213 O_3 near the surface in NCP in hazy days. The photolysis of nitrate had a limited
1214 impact on nitrate concentrations (reduced by $<5\%$ with $J_{\text{nitrate}}/J_{\text{HNO}_3} = 30$, and $<15\%$
1215 even with a $J_{\text{nitrate}}/J_{\text{HNO}_3}$ ratio of 120), due mainly to the simultaneously enhanced
1216 atmospheric oxidants favoring the formation of HNO_3 and nitrate. Choosing a larger
1217 J_{nitrate} value might cover up other ground-based unknown HONO sources, but

Deleted: oxidation

Deleted:

Deleted: formation

Formatted: Subscript

1222 overestimate vertical sources of HONO, and NO_x and O₃ concentrations, so more
1223 studies are still needed to find the exact value of J_{nitrate} in the real atmosphere.

1224

1225 **Data availability**

1226 Data are available upon reasonable request to the corresponding authors.

1227

1228 **Author contribution:**

1229 J.Z., C.L., J.A., M.G., and W.W. conceived and designed the research. J.Z. performed

1230 WRF-Chem simulations and wrote the paper. J.Z., C.L., Y.G., and H.R. performed

Deleted: and analyzed

1231 data analyses and produced the figures. C.L., Y.Z., F.Z., X.F., C.Y., K.D., Y.L., and

1232 M.K. conducted the field observations. W.W., J.A., M.G., Y.L., and M.K. reviewed the

Deleted: .

1233 article.

1234 **Competing interests**

1235 The authors declare that they have no conflict of interest.

1236

1237 **Acknowledgements**

1238 This research was partially supported by the National Natural Science Foundation of

1239 China (Grant No. 92044302, 42075108, 42107124, [42075110](#), 41822703, 91544221,

1240 91844301), Beijing National Laboratory for Molecular Sciences

1243 (BNLMS-CXXM-202011) and the China Postdoctoral Science Foundation (grant NO.

1244 2019M660764).

1245

1246 **References**

- 1247 Aliche, B., Platt, U., Stutz, J., 2002. Impact of nitrous acid photolysis on the total hydroxyl radical
 1248 budget during the Limitation of Oxidant Production/Pianura Padana Produzione di Ozono study in
 1249 Milan. *J Geophys Res-Atmos* 107. doi:10.1029/2000JD000075.
- 1250 An, J.L., Li, Y., Chen, Y., Li, J., Qu, Y., Tang, Y.J., 2013. Enhancements of major aerosol components
 1251 due to additional HONO sources in the North China Plain and implications for visibility and haze.
 1252 *Advances in Atmospheric Sciences* 30, 57-66.
- 1253 [Aumont, B., Chervier, F., Laval, S., 2003. Contribution of HONO sources to the NO_x/HO_x/O₃
 1254 chemistry in the polluted boundary layer. *Atmospheric Environment* 37, 487-498.](#)
- 1255 Avnery, S., Mauzerall, D.L., Liu, J., Horowitz, L.W., 2011a. Global crop yield reductions due to surface
 1256 ozone exposure: 1. Year 2000 crop production losses and economic damage. *Atmospheric*
 1257 *Environment* 45, 2284-2296.
- 1258 Avnery, S., Mauzerall, D.L., Liu, J., Horowitz, L.W., 2011b. Global crop yield reductions due to
 1259 surface ozone exposure: 2. Year 2030 potential crop production losses and economic damage
 1260 under two scenarios of O₃ pollution. *Atmospheric Environment* 45, 2297-2309.
- 1261 Baergen, A.M., Donaldson, D.J., 2013. Photochemical renoxification of nitric acid on real urban grime.
 1262 *Environmental Science & Technology* 47, 815-820.
- 1263 Bao, F., Li, M., Zhang, Y., Chen, C., Zhao, J., 2018. Photochemical Aging of Beijing Urban PM_{2.5}:
 1264 HONO Production. *Environmental Science & Technology* 52, 6309-6316.
- 1265 Bao, F.X., Jiang, H.Y., Zhang, Y., Li, M., Ye, C.X., Wang, W.G., Ge, M.F., Chen, C.C., Zhao, J.C., 2020.
 1266 The Key Role of Sulfate in the Photochemical Renoxification on Real PM_{2.5}. *Environmental*
 1267 *Science & Technology* 54, 3121-3128.
- 1268 [Bejan, I., Abd-el-Aal, Y., Barnes, I., Benter, T., Bohn, B., Wiesen, P., Kleffmann, J., 2006. The
 1269 photolysis of ortho-nitrophenols: a new gas phase source of HONO. *Physical chemistry chemical*
 1270 *physics : PCCP* 8, 2028-2035.](#)
- 1271 Chen, S., Wang, H., Lu, K., Zeng, L., Hu, M., Zhang, Y., 2020a. The trend of surface ozone in Beijing
 1272 from 2013 to 2019: Indications of the persisting strong atmospheric oxidation capacity.
 1273 *Atmospheric Environment* 242, 117801.
- 1274 Chen, Y., Wang, W.G., Lian, C.F., Peng, C., Zhang, W.Y., Li, J.L., Liu, M.Y., Shi, B., Wang, X.F., Ge,
 1275 M.F., 2020b. Evaluation and impact factors of indoor and outdoor gas-phase nitrous acid under
 1276 different environmental conditions. *Journal of Environmental Sciences* 95, 165-171.
- 1277 [Chen, Y., Zheng, P., Wang, Z., Pu, W., Tan, Y., Yu, C., Xia, M., Wang, W., Guo, J., Huang, D., Yan, C.,
 1278 Nie, W., Ling, Z., Chen, Q., Lee, S., Wang, T., 2021. Secondary Formation and Impacts of
 1279 Gaseous Nitro-Phenolic Compounds in the Continental Outflow Observed at a Background Site in
 1280 South China. *Environmental Science & Technology*. DOI: 10.1021/acs.est.1c04596.](#)
- 1281 [Crowley, J.N., Carl, S.A., 1997. OH formation in the photoexcitation of NO₂ beyond the dissociation
 1282 threshold in the presence of water vapor. *Journal of Physical Chemistry A* 101, 4178-4184.](#)
- 1283 Cui, L., Li, R., Fu, H., Meng, Y., Zhao, Y., Li, Q., Chen, J., 2021. Nitrous acid emission from open
 1284 burning of major crop residues in mainland China. *Atmospheric Environment* 244, 117950.
- 1285 [Dillon, T.J., Crowley, J.N., 2018. Reactive quenching of electronically excited NO_x^{*} and NO_x^{*} by H₂O
 1286 as potential sources of atmospheric HO_x radicals. *Atmospheric Chemistry and Physics* 18,
 1287 14005-14015.](#)

Formatted: Subscript

Formatted: Subscript

Formatted: Subscript

Formatted: Subscript

Formatted: Superscript

Formatted: Subscript

Formatted: Superscript

Formatted: Subscript

Formatted: Subscript

- 1288 Dong, W., Xing, J., Wang, S., 2010. Temporal and spatial distribution of anthropogenic ammonia
1289 emissions in China: 1994-2006. *Environmental Sciences (in Chinese)* 31, 1457-1463.
- 1290 [Emmons, L.K., Walters, S., Hess, P.G., Lamarque, J.F., Pfister, G.G., Fillmore, D., Granier, C.,](#)
1291 [Guenther, A., Kinnison, D., Laepple, T., Orlando, J., Tie, X., Tyndall, G., Wiedinmyer, C.,](#)
1292 [Baughcum, S.L., Kloster, S., 2010. Description and evaluation of the Model for Ozone and](#)
1293 [Related chemical Tracers, version 4 \(MOZART-4\). *Geoscientific Model Development* 3, 43-67.](#)
- 1294 Feng, T., Zhao, S., Bei, N., Liu, S., Li, G., 2021. Increasing atmospheric oxidizing capacity weakens
1295 emission mitigation effort in Beijing during autumn haze events. *Chemosphere* 281, 130855.
- 1296 Feng, Z., De Marco, A., Anav, A., Gualtieri, M., Sicard, P., Tian, H., Formasier, F., Tao, F., Guo, A.,
1297 Paoletti, E., 2019. Economic losses due to ozone impacts on human health, forest productivity and
1298 crop yield across China. *Environ Int* 131, 104966.
- 1299 Feng, Z., Hu, E., Wang, X., Jiang, L., Liu, X., 2015. Ground-level O₃ pollution and its impacts on food
1300 crops in China: a review. *Environ Pollut* 199, 42-48.
- 1301 [Feng, Z., Xu, Y., Kobayashi, K., Dai, L., Zhang, T., Agathokleous, E., Calatayud, V., Paoletti, E.,](#)
1302 [Mukherjee, A., Agrawal, M., Park, R.J., Oak, Y.J., Yue, X., 2022. Ozone pollution threatens the](#)
1303 [production of major staple crops in East Asia. *Nature Food* 3, 47-56.](#)
- 1304 Finlayson-Pitts, B.J., Wingen, L.M., Sumner, A.L., Syomin, D., Ramazan, K.A., 2003. The
1305 heterogeneous hydrolysis of NO₂ in laboratory systems and in outdoor and indoor atmospheres:
1306 An integrated mechanism. *Physical Chemistry Chemical Physics* 5, 223-242.
- 1307 [Fröhlich, R., Cubison, M.J., Slowik, J.G., Bukowiecki, N., Prévôt, A.S.H., Baltensperger, U., Schneider,](#)
1308 [J., Kimmel, J.R., Gonin, M., Rohner, U., Worsnop, D.R., Jayne, J.T., 2013. The ToF-ACSM: a](#)
1309 [portable aerosol chemical speciation monitor with TOFMS detection. *Atmospheric Measurement*](#)
1310 [Techniques 6, 3225-3241.](#)
- 1311 Fu, X., Wang, T., Gao, J., Wang, P., Liu, Y.M., Wang, S.X., Zhao, B., Xue, L.K., 2020. Persistent Heavy
1312 Winter Nitrate Pollution Driven by Increased Photochemical Oxidants in Northern China.
1313 *Environmental Science & Technology* 54, 3881-3889.
- 1314 Fu, X., Wang, T., Zhang, L., Li, Q.Y., Wang, Z., Xia, M., Yun, H., Wang, W.H., Yu, C., Yue, D.L., Zhou,
1315 Y., Zheng, J.Y., Han, R., 2019. The significant contribution of HONO to secondary pollutants
1316 during a severe winter pollution event in southern China. *Atmospheric Chemistry and Physics* 19,
1317 1-14.
- 1318 Gao, W., Tan, G., Hong, Y., Li, M., Nian, H., Guo, C., Huang, Z., Fu, Z., Dong, J., Xu, X., 2013.
1319 Development of portable single photon ionization time-of-flight mass spectrometer combined with
1320 membrane inlet. *International Journal of Mass Spectrometry* 334, 8-12.
- 1321 Ge, M., Tong, S., Wang, W., Zhang, W., Chen, M., Peng, C., Li, J., Zhou, L., Chen, Y., Liu, M., 2021.
1322 Important Oxidants and Their Impact on the Environmental Effects of Aerosols. *The journal of*
1323 *physical chemistry. A* 125, 3813-3825.
- 1324 Ge, S., Wang, G., Zhang, S., Li, D., Xie, Y., Wu, C., Yuan, Q., Chen, J., Zhang, H., 2019. Abundant
1325 NH₃ in China Enhances Atmospheric HONO Production by Promoting the Heterogeneous
1326 Reaction of SO₂ with NO₂. *Environmental Science & Technology* 53, 14339-14347.
- 1327 [Gen, M., Liang, Z., Zhang, R., Go Mabato, B.R., Chan, C.K., 2022. Particulate nitrate photolysis in the](#)
1328 [atmosphere. *Environmental Science: Atmospheres*. DOI: 10.1039/D1EA00087J.](#)
- 1329 Gligorovski, S., Strekowski, R., Barbati, S., Vione, D., 2015. Environmental Implications of Hydroxyl
1330 Radicals (*OH). *Chem Rev* 115, 13051-13092.
- 1331 Gómez Alvarez, E., Sörgel, M., Gligorovski, S., Bassil, S., Bartolomei, V., Coulomb, B., Zetzsch, C.,

Formatted: Normal, Indent: Left: 0 cm, Hanging: 4.2 ch,
First line: 0 ch

Formatted: Normal, Indent: Left: 0 cm, Hanging: 4.2 ch,
First line: 0 ch

1332 Wortham, H., 2014. Light-induced nitrous acid (HONO) production from NO₂ heterogeneous
1333 reactions on household chemicals. *Atmospheric Environment* 95, 391-399.

1334 Guenther, A.B., Jiang, X., Heald, C.L., Sakulyanontvittaya, T., Duhl, T., Emmons, L.K., Wang, X.,
1335 2012. The Model of Emissions of Gases and Aerosols from Nature version 2.1 (MEGAN2.1): an
1336 extended and updated framework for modeling biogenic emissions. *Geoscientific Model*
1337 *Development* 5, 1471-1492.

1338 Guo, Y., Zhang, J., An, J., Qu, Y., Liu, X., Sun, Y., Chen, Y., 2020. Effect of vertical parameterization of
1339 a missing daytime source of HONO on concentrations of HONO, O₃ and secondary organic
1340 aerosols in eastern China. *Atmospheric Environment* 226, 117208.

1341 Hendrick, F., Muller, J.F., Clemer, K., Wang, P., De Maziere, M., Fayt, C., Gielen, C., Hermans, C., Ma,
1342 J.Z., Pinardi, G., Stavrou, T., Vlemmix, T., Van Roozendaal, M., 2014. Four years of
1343 ground-based MAX-DOAS observations of HONO and NO₂ in the Beijing area. *Atmospheric*
1344 *Chemistry and Physics* 14, 765-781.

1345 Huang, X., Li, M.M., Li, J.F., Song, Y., 2012. A high-resolution emission inventory of crop burning in
1346 fields in China based on MODIS Thermal Anomalies/Fire products. *Atmospheric Environment* 50,
1347 9-15.

1348 Kasibhatla, P., Sherwen, T., Evans, M.J., Carpenter, L.J., Reed, C., Alexander, B., Chen, Q.J., Sulprizio,
1349 M.P., Lee, J.D., Read, K.A., Bloss, W., Crilley, L.R., Keene, W.C., Pszenny, A.A.P., Hodzic, A.,
1350 2018. Global impact of nitrate photolysis in sea-salt aerosol on NO_x, OH, and O₃ in the marine
1351 boundary layer. *Atmospheric Chemistry and Physics* 18, 11185-11203.

1352 Kim, S., VandenBoer, T.C., Young, C.J., Riedel, T.P., Thornton, J.A., Swarthout, B., Sive, B., Lerner, B.,
1353 Gilman, J.B., Warneke, C., Roberts, J.M., Guenther, A., Wagner, N.L., Dube, W.P., Williams, E.,
1354 Brown, S.S., 2014. The primary and recycling sources of OH during the NACHTT-2011
1355 campaign: HONO as an important OH primary source in the wintertime. *J Geophys Res-Atmos*
1356 119, 6886-6896.

1357 Kleffmann, J., Kurtenbach, R., Lorzer, J., Wiesen, P., Kalthoff, N., Vogel, B., Vogel, H., 2003.
1358 Measured and simulated vertical profiles of nitrous acid - Part I: Field measurements.
1359 *Atmospheric Environment* 37, 2949-2955.

1360 Klosterkother, A., Kurtenbach, R., Wiesen, P., Kleffmann, J., 2021. Determination of the emission
1361 indices for NO, NO₂, HONO, HCHO, CO, and particles emitted from candles. *Indoor Air* 31,
1362 116-127.

1363 Kramer, L.J., Crilley, L.R., Adams, T.J., Ball, S.M., Pope, F.D., Bloss, W.J., 2020. Nitrous acid (HONO)
1364 emissions under real-world driving conditions from vehicles in a UK road tunnel. *Atmospheric*
1365 *Chemistry and Physics* 20, 5231-5248.

1366 Kubota, M., Asami, T., 1985. Volatilization of Nitrous-Acid from Upland Soils. *Soil Science and Plant*
1367 *Nutrition* 31, 27-34.

1368 Kurtenbach, R., Becker, K.H., Gomes, J.A.G., Kleffmann, J., Lorzer, J.C., Spittler, M., Wiesen, P.,
1369 Ackermann, R., Geyer, A., Platt, U., 2001. Investigations of emissions and heterogeneous
1370 formation of HONO in a road traffic tunnel. *Atmospheric Environment* 35, 3385-3394.

1371 Laufs, S., Kleffmann, J., 2016. Investigations on HONO formation from photolysis of adsorbed HNO₃
1372 on quartz glass surfaces. *Physical Chemistry Chemical Physics* 18, 9616-9625.

1373 [Lee, J.D., Whalley, L.K., Heard, D.E., Stone, D., Dunmore, R.E., Hamilton, J.F., Young, D.E., Allan,](#)
1374 [J.D., Laufs, S., Kleffmann, J., 2016. Detailed budget analysis of HONO in central London reveals](#)
1375 [a missing daytime source. *Atmospheric Chemistry and Physics* 16, 2747-2764.](#)

- 1376 Li, G., Lei, W., Zavala, M., Volkamer, R., Dusanter, S., Stevens, P., Molina, L.T., 2010. Impacts of
1377 HONO sources on the photochemistry in Mexico City during the MCMA-2006/MILAGO
1378 Campaign. *Atmospheric Chemistry and Physics* 10, 6551-6567.
- 1379 Li, K., Jacob, D.J., Shen, L., Lu, X., De Smedt, I., Liao, H., 2020. Increases in surface ozone pollution
1380 in China from 2013 to 2019: anthropogenic and meteorological influences. *Atmospheric*
1381 *Chemistry and Physics* 20, 11423-11433.
- 1382 Li, L., Chen, C.H., Huang, C., Huang, H.Y., Zhang, G.F., Wang, Y.J., Wang, H.L., Lou, S.R., Qiao, L.P.,
1383 Zhou, M., Chen, M.H., Chen, Y.R., Streets, D.G., Fu, J.S., Jang, C.J., 2012. Process analysis of
1384 regional ozone formation over the Yangtze River Delta, China using the Community Multi-scale
1385 Air Quality modeling system. *Atmospheric Chemistry and Physics* 12, 10971-10987.
- 1386 Li, M., Zhang, Q., Kurokawa, J., Woo, J.H., He, K.B., Lu, Z.F., Ohara, T., Song, Y., Streets, D.G.,
1387 Carmichael, G.R., Cheng, Y.F., Hong, C.P., Huo, H., Jiang, X.J., Kang, S.C., Liu, F., Su, H., Zheng,
1388 B., 2017. MIX: a mosaic Asian anthropogenic emission inventory under the international
1389 collaboration framework of the MICS-Asia and HTAP. *Atmospheric Chemistry and Physics* 17,
1390 935-963.
- 1391 [Li, S., Matthews, J., Sinha, A., 2008. Atmospheric hydroxyl radical production from electronically](#)
1392 [excited NO₂ and H₂O. *Science* 319, 1657-1660.](#)
- 1393 [Li, X., Rohrer, F., Hofzumahaus, A., Brauers, T., Häsel, R., Bohn, B., Broch, S., Fuchs, H., Gomm, S.,](#)
1394 [Holland, F., 2015. Response to Comment on “Missing gas-phase source of HONO inferred from](#)
1395 [Zeppelin measurements in the troposphere”. *Science* 348, 1326-1326.](#)
- 1396 [Li, X., Rohrer, F., Hofzumahaus, A., Brauers, T., Haseler, R., Bohn, B., Broch, S., Fuchs, H., Gomm, S.,](#)
1397 [Holland, F., Jäger, J., Kaiser, J., Keutsch, F.N., Lohse, I., Lu, K., Tillmann, R., Wegener, R., Wolfe,](#)
1398 [G.M., Mentel, T.F., Kiendler-Scharr, A., Wahner, A., 2014. Missing gas-phase source of HONO](#)
1399 [inferred from Zeppelin measurements in the troposphere. *Science* 344, 292-296.](#)
- 1400 Li, Y., An, J.L., Min, M., Zhang, W., Wang, F., Xie, P.H., 2011. Impacts of HONO sources on the air
1401 quality in Beijing, Tianjin and Hebei Province of China. *Atmospheric Environment* 45,
1402 4735-4744.
- 1403 Liao, S., Zhang, J., Yu, F., Zhu, M., Liu, J., Ou, J., Dong, H., Sha, Q., Zhong, Z., Xie, Y., Luo, H.,
1404 Zhang, L., Zheng, J., 2021. High Gaseous Nitrous Acid (HONO) Emissions from Light-Duty
1405 Diesel Vehicles. *Environmental science & technology* 55, 200-208.
- 1406 Lin, Y.L., Farley, R.D., Orville, H.D., 1983. Bulk Parameterization of the Snow Field in a Cloud Model.
1407 *J Clim Appl Meteorol* 22, 1065-1092.
- 1408 Liu, J., Li, S., Zeng, J., Mekic, M., Yu, Z., Zhou, W., Loisel, G., Gandolfo, A., Song, W., Wang, X.,
1409 Zhou, Z., Herrmann, H., Li, X., Gligorovski, S., 2019. Assessing indoor gas phase oxidation
1410 capacity through real-time measurements of HONO and NO_x in Guangzhou, China. *Environ Sci*
1411 *Process Impacts* 21, 1393-1402.
- 1412 [Liu, Y., Zhang, Y., Lian, C., Yan, C., Feng, Z., Zheng, F., Fan, X., Chen, Y., Wang, W., Chu, B., Wang,](#)
1413 [Y., Cai, J., Du, W., Daellenbach, K.R., Kangasluoma, J., Bianchi, F., Kujansuu, J., Petäjä, T., Wang,](#)
1414 [X., Hu, B., Wang, Y., Ge, M., He, H., Kulmala, M., 2020. The promotion effect of nitrous acid on](#)
1415 [aerosol formation in wintertime in Beijing: the possible contribution of traffic-related emissions.](#)
1416 [*Atmospheric Chemistry and Physics* 20, 13023-13040.](#)
- 1417 Liu, Z., Wang, Y., Costabile, F., Amoroso, A., Zhao, C., Huey, L.G., Stickel, R., Liao, J., Zhu, T., 2014.
1418 Evidence of aerosols as a media for rapid daytime HONO production over China. *Environmental*
1419 *Science & Technology* 48, 14386-14391.

Formatted: Subscript

Formatted: Subscript

- 1420 Lu, X., Zhang, L., Wang, X.L., Gao, M., Li, K., Zhang, Y.Z., Yue, X., Zhang, Y.H., 2020. Rapid
1421 Increases in Warm-Season Surface Ozone and Resulting Health Impact in China Since 2013.
1422 Environmental Science & Technology Letters 7, 240-247.
- 1423 Ma, J., Liu, Y., Han, C., Ma, Q., Liu, C., He, H., 2013. Review of heterogeneous photochemical
1424 reactions of NO_x on aerosol — A possible daytime source of nitrous acid (HONO) in the
1425 atmosphere. Journal of Environmental Sciences 25, 326-334.
- 1426 Ma, Z.Q., Xu, J., Quan, W.J., Zhang, Z.Y., Lin, W.L., Xu, X.B., 2016. Significant increase of surface
1427 ozone at a rural site, north of eastern China. Atmospheric Chemistry and Physics 16, 3969-3977.
- 1428 Maji, K.J., Namdeo, A., 2021. Continuous increases of surface ozone and associated premature
1429 mortality growth in China during 2015-2019. Environ Pollut 269, 116183.
- 1430 Marion, A., Morin, J., Gandolfo, A., Ormeno, E., D'Anna, B., Wortham, H., 2021. Nitrous acid
1431 formation on Zea mays leaves by heterogeneous reaction of nitrogen dioxide in the laboratory.
1432 Environ Res 193, 110543.
- 1433 Meng, F.H., Qin, M., Tang, K., Duan, J., Fang, W., Liang, S.X., Ye, K.D., Xie, P.H., Sun, Y.L., Xie,
1434 C.H., Ye, C.X., Fu, P.Q., Liu, J.G., Liu, W.Q., 2020. High-resolution vertical distribution and
1435 sources of HONO and NO_2 in the nocturnal boundary layer in urban Beijing, China. Atmospheric
1436 Chemistry and Physics 20, 5071-5092.
- 1437 Mills, G., Buse, A., Gimeno, B., Bermejo, V., Holland, M., Emberson, L., Pleijel, H., 2007. A synthesis
1438 of AOT40-based response functions and critical levels of ozone for agricultural and horticultural
1439 crops. Atmospheric Environment 41, 2630-2643.
- 1440 Mills, G., Sharps, K., Simpson, D., Pleijel, H., Broberg, M., Uddling, J., Jaramillo, F., Davies, W.J.,
1441 Dentener, F., Van den Berg, M., Agrawal, M., Agrawal, S.B., Ainsworth, E.A., Buker, P.,
1442 Emberson, L., Feng, Z., Harmens, H., Hayes, F., Kobayashi, K., Paoletti, E., Van Dingenen, R.,
1443 2018. Ozone pollution will compromise efforts to increase global wheat production. Glob Chang
1444 Biol 24, 3560-3574.
- 1445 Oswald, R., Behrendt, T., Ermel, M., Wu, D., Su, H., Cheng, Y., Breuninger, C., Moravek, A., Mougín,
1446 E., Delon, C., Loubet, B., Pommerening-Roser, A., Sorgel, M., Poschl, U., Hoffmann, T., Andreae,
1447 M.O., Meixner, F.X., Trebs, I., 2013. HONO emissions from soil bacteria as a major source of
1448 atmospheric reactive nitrogen. Science 341, 1233-1235.
- 1449 [Pagsberg, P., Bjergbakke, E., Ratajczak, E., Silleesen, A., 1997. Kinetics of the gas phase reaction](#)
1450 [OH+NO \(+M\)->HONO \(+M\) and the determination of the UV absorption cross sections of](#)
1451 [HONO. Chemical Physics Letters 272, 383-390.](#)
- 1452 Perner, D., Platt, U., 1979. Detection of nitrous acid in the atmosphere by differential optical absorption.
1453 Geophysical Research Letters 6, 917-920.
- 1454 Pitts, J.N., Wallington, T.J., Biermann, H.W., Winer, A.M., 1985. Identification and Measurement of
1455 Nitrous-Acid in an Indoor Environment. Atmospheric Environment 19, 763-767.
- 1456 [Qu, Y., Chen, Y., Liu, X., Zhang, J., Guo, Y., An, J., 2019. Seasonal effects of additional HONO sources](#)
1457 [and the heterogeneous reactions of \$\text{N}_2\text{O}_5\$ on nitrate in the North China Plain. The Science of the](#)
1458 [total environment 690, 97-107.](#)
- 1459 Reed, C., Evans, M.J., Crilley, L.R., Bloss, W.J., Sherwen, T., Read, K.A., Lee, J.D., Carpenter, L.J.,
1460 2017. Evidence for renoxification in the tropical marine boundary layer. Atmospheric Chemistry
1461 and Physics 17, 4081-4092.
- 1462 Richards, B.L., Middleton, J.T., Hewitt, W.B., 1958. Air Pollution With Relation to Agronomic Crops:
1463 V. Oxidant Stipple of Grape. Agronomy Journal 50, 559-561.

Formatted: Subscript

Formatted: Subscript

Formatted: Subscript

1464 Rohrer, F., Bohn, B., Brauers, T., Bruning, D., Johnen, F.J., Wahner, A., Kleffmann, J., 2005.
1465 Characterisation of the photolytic HONO-source in the atmosphere simulation chamber SAPHIR.
1466 Atmospheric Chemistry and Physics 5, 2189-2201.

1467 Romer, P.S., Wooldridge, P.J., Crouse, J.D., Kim, M.J., Wennberg, P.O., Dibb, J.E., Scheuer, E., Blake,
1468 D.R., Meinardi, S., Brosius, A.L., Thames, A.B., Miller, D.O., Brune, W.H., Hall, S.R., Ryerson,
1469 T.B., Cohen, R.C., 2018. Constraints on Aerosol Nitrate Photolysis as a Potential Source of
1470 HONO and NO_x . *Environmental Science & Technology* 52, 13738-13746.

1471 Rondon, A., Sanhueza, E., 1989. High HONO atmospheric concentrations during vegetation burning in
1472 the tropical savannah. *Tellus Ser. B-Chem. Phys. Meteorol.* 41, 474-477.

1473 Ryan, R.G., Rhodes, S., Tully, M., Wilson, S., Jones, N., Friess, U., Schofield, R., 2018. Daytime
1474 HONO, NO_2 and aerosol distributions from MAX-DOAS observations in Melbourne.
1475 Atmospheric Chemistry and Physics 18, 13969-13985.

1476 [Saliba, N.A., Mochida, M., Finlayson-Pitts, B.J., 2000. Laboratory studies of sources of HONO in
1477 polluted urban atmospheres. *Geophysical Research Letters* 27, 3229-3232.](#)

1478 Sakamaki, F., Hatakeyama, S., Akimoto, H., 1983. Formation of Nitrous-Acid and Nitric-Oxide in the
1479 Heterogeneous Dark Reaction of Nitrogen-Dioxide and Water-Vapor in a Smog Chamber.
1480 International Journal of Chemical Kinetics 15, 1013-1029.

1481 Sarwar, G., Roselle, S.J., Mathur, R., Appel, W., Dennis, R.L., Vogel, B., 2008. A comparison of
1482 CMAQ HONO predictions with observations from the northeast oxidant and particle study.
1483 Atmospheric Environment 42, 5760-5770.

1484 Selin, N.E., Wu, S., Nam, K.M., Reilly, J.M., Paltsev, S., Prinn, R.G., Webster, M.D., 2009. Global
1485 health and economic impacts of future ozone pollution. *Environmental Research Letters* 4,
1486 044014.

1487 Shi, Q., Tao, Y., Krechmer, J.E., Heald, C.L., Murphy, J.G., Kroll, J.H., Ye, Q., 2021. Laboratory
1488 Investigation of Renoxification from the Photolysis of Inorganic Particulate Nitrate.
1489 *Environmental science & technology*. 55, 854–861.

1490 Shi, X., Ge, Y., Zheng, J., Ma, Y., Ren, X., Zhang, Y., 2020. Budget of nitrous acid and its impacts on
1491 atmospheric oxidative capacity at an urban site in the central Yangtze River Delta region of China.
1492 Atmospheric Environment 238, 117725.

1493 Sillman, S., 1995. The use of NO_y , H_2O_2 , and HNO_3 as indicators for ozone- NO_x -hydrocarbon
1494 sensitivity in urban locations. *Journal of Geophysical Research: Atmospheres* 100, 14175-14188.

1495 Slater, E.J., Whalley, L.K., Woodward-Massey, R., Ye, C.X., Lee, J.D., Squires, F., Hopkins, J.R.,
1496 Dunmore, R.E., Shaw, M., Hamilton, J.F., Lewis, A.C., Crilley, L.R., Kramer, L., Bloss, W., Vu, T.,
1497 Sun, Y.L., Xu, W.Q., Yue, S.Y., Ren, L.J., Acton, W.J.F., Hewitt, C.N., Wang, X.M., Fu, P.Q.,
1498 Heard, D.E., 2020. Elevated levels of OH observed in haze events during wintertime in central
1499 Beijing. *Atmospheric Chemistry and Physics* 20, 14847-14871.

1500 Sorgel, M., Trebs, I., Serafimovich, A., Moravek, A., Held, A., Zetzsch, C., 2011. Simultaneous HONO
1501 measurements in and above a forest canopy: influence of turbulent exchange on mixing ratio
1502 differences. *Atmospheric Chemistry and Physics* 11, 841-855.

1503 [Stuhl, F., Niki, H., 1972. Flash Photochemical Study of the Reaction \$\text{OH}+\text{NO}+\text{M}\$ Using Resonance
1504 Fluorescent Detection of OH. *The Journal of Chemical Physics* 57, 3677-3679.](#)

1505 Tan, Z.F., Rohrer, F., Lu, K.D., Ma, X.F., Bohn, B., Broch, S., Dong, H.B., Fuchs, H., Gkatzelis, G.I.,
1506 Hofzumahaus, A., Holland, F., Li, X., Liu, Y., Liu, Y.H., Novelli, A., Shao, M., Wang, H.C., Wu,
1507 Y.S., Zeng, L.M., Hu, M., Kiendler-Scharr, A., Wahner, A., Zhang, Y.H., 2018. Wintertime

Formatted: Subscript

Deleted: .

- 1509 photochemistry in Beijing: observations of RO_x radical concentrations in the North China Plain
1510 during the BEST-ONE campaign. *Atmospheric Chemistry and Physics* 18, 12391-12411.
- 1511 Tang, M.J., Huang, X., Lu, K.D., Ge, M.F., Li, Y.J., Cheng, P., Zhu, T., Ding, A.J., Zhang, Y.H.,
1512 Gligorovski, S., Song, W., Ding, X., Bi, X.H., Wang, X.M., 2017. Heterogeneous reactions of
1513 mineral dust aerosol: implications for tropospheric oxidation capacity. *Atmospheric Chemistry and*
1514 *Physics* 17, 11727-11777.
- 1515 Tang, Y., An, J., Wang, F., Li, Y., Qu, Y., Chen, Y., Lin, J., 2015. Impacts of an unknown daytime
1516 HONO source on the mixing ratio and budget of HONO, and hydroxyl, hydroperoxyl, and organic
1517 peroxy radicals, in the coastal regions of China. *Atmospheric Chemistry and Physics* 15,
1518 9381-9398.
- 1519 Theys, N., Volkamer, R., Mueller, J.F., Zarzana, K.J., Kille, N., Clarisse, L., De Smedt, I., Lerot, C.,
1520 Finkenzeller, H., Hendrick, F., Koenig, T.K., Lee, C.F., Knote, C., Yu, H., Van Roozendael, M.,
1521 2020. Global nitrous acid emissions and levels of regional oxidants enhanced by wildfires. *Nature*
1522 *Geoscience* 13, 681-686.
- 1523 Tie, X., Long, X., Li, G., Zhao, S., Cao, J., Xu, J., 2019. Ozone enhancement due to the
1524 photodissociation of nitrous acid in eastern China. *Atmospheric Chemistry and Physics* 19,
1525 11267-11278.
- 1526 VandenBoer, T.C., Brown, S.S., Murphy, J.G., Keene, W.C., Young, C.J., Pszenny, A.A.P., Kim, S.,
1527 Warneke, C., de Gouw, J.A., Maben, J.R., Wagner, N.L., Riedel, T.P., Thornton, J.A., Wolfe, D.E.,
1528 Dube, W.P., Ozturk, F., Brock, C.A., Grossberg, N., Lefer, B., Lerner, B., Middlebrook, A.M.,
1529 Roberts, J.M., 2013. Understanding the role of the ground surface in HONO vertical structure:
1530 High resolution vertical profiles during NACHTT-11. *J Geophys Res-Atmos* 118, 10155-10171.
- 1531 Villena, G., Kleffmann, J., Kurtenbach, R., Wiesen, P., Lissi, E., Rubio, M.A., Croxatto, G.,
1532 Rappenglück, B., 2011. Vertical gradients of HONO, NO_x and O₃ in Santiago de Chile.
1533 *Atmospheric Environment* 45, 3867-3873.
- 1534 Wang, F., An, J.L., Li, Y., Tang, Y.J., Lin, J., Qu, Y., Chen, Y., Zhang, B., Zhai, J., 2014. Impacts of
1535 uncertainty in AVOC emissions on the summer RO_x budget and ozone production rate in the three
1536 most rapidly-developing economic growth regions of China. *Advances in Atmospheric Sciences*
1537 31, 1331-1342.
- 1538 Wang, X., Zhang, Y., Hu, Y., Zhou, W., Lu, K., Zhong, L., Zeng, L., Shao, M., Hu, M., Russell, A.G.,
1539 2010. Process analysis and sensitivity study of regional ozone formation over the Pearl River
1540 Delta, China, during the PRIDE-PRD2004 campaign using the Community Multiscale Air Quality
1541 modeling system. *Atmospheric Chemistry and Physics* 10, 4423-4437.
- 1542 Wang, Y., Apituley, A., Bais, A., Beirle, S., Benavent, N., Borovski, A., Bruchkouski, I., Chan, K.L.,
1543 Donner, S., Drosoglou, T., Finkenzeller, H., Friedrich, M.M., Friess, U., Garcia-Nieto, D.,
1544 Gomez-Martin, L., Hendrick, F., Hilboll, A., Jin, J.L., Johnston, P., Koenig, T.K., Kreher, K.,
1545 Kumar, V., Kyuberis, A., Lampel, J., Liu, C., Liu, H.R., Ma, J.Z., Polyansky, O.L., Postlyakov,
1546 O., Querel, R., Saiz-Lopez, A., Schmitt, S., Tian, X., Tirpitz, J.L., Van Roozendael, M., Volkamer,
1547 R., Wang, Z.R., Xie, P.H., Xing, C.Z., Xu, J., Yela, M., Zhang, C.X., Wagner, T., 2020.
1548 Inter-comparison of MAX-DOAS measurements of tropospheric HONO slant column densities
1549 and vertical profiles during the CINDI-2 campaign. *Atmospheric Measurement Techniques* 13,
1550 5087-5116.
- 1551 Wang, Y., Dörner, S., Donner, S., Böhnke, S., De Smedt, I., Dickerson, R.R., Dong, Z., He, H., Li, Z.,
1552 Li, Z., Li, D., Liu, D., Ren, X., Theys, N., Wang, Y., Wang, Y., Wang, Z., Xu, H., Xu, J., Wagner,

1553 T., 2019. Vertical profiles of NO₂, SO₂, HONO, HCHO, CHOCHO and aerosols derived from
1554 MAX-DOAS measurements at a rural site in the central western North China Plain and their
1555 relation to emission sources and effects of regional transport. *Atmospheric Chemistry and Physics*
1556 19, 5417-5449.

1557 Wilkinson, S., Mills, G., Illidge, R., Davies, W.J., 2012. How is ozone pollution reducing our food
1558 supply? *J Exp Bot* 63, 527-536.

1559 Wong, K.W., Oh, H.J., Lefer, B.L., Rappengluck, B., Stutz, J., 2011. Vertical profiles of nitrous acid in
1560 the nocturnal urban atmosphere of Houston, TX. *Atmospheric Chemistry and Physics* 11,
1561 3595-3609.

1562 Wong, K.W., Tsai, C., Lefer, B., Haman, C., Grossberg, N., Brune, W.H., Ren, X., Luke, W., Stutz, J.,
1563 2012. Daytime HONO vertical gradients during SHARP 2009 in Houston, TX. *Atmospheric*
1564 *Chemistry and Physics* 12, 635-652.

1565 Wu, D., Horn, M.A., Behrendt, T., Muller, S., Li, J., Cole, J.A., Xie, B., Ju, X., Li, G., Ermel, M.,
1566 Oswald, R., Frohlich-Nowoisky, J., Hoor, P., Hu, C., Liu, M., Andreae, M.O., Poschl, U., Cheng,
1567 Y., Su, H., Trebs, I., Weber, B., Sorgel, M., 2019. Soil HONO emissions at high moisture content
1568 are driven by microbial nitrate reduction to nitrite: tackling the HONO puzzle. *ISME J* 13,
1569 1688-1699.

1570 Xing, C., Liu, C., Hu, Q., Fu, Q., Wang, S., Lin, H., Zhu, Y., Wang, S., Wang, W., Javed, Z., 2021.
1571 Vertical distributions of wintertime atmospheric nitrogenous compounds and the corresponding
1572 OH radicals production in Leshan, southwest China. *Journal of Environmental Sciences* 105,
1573 44-55.

1574 Xing, L., Wu, J.R., Elser, M., Tong, S.R., Liu, S.X., Li, X., Liu, L., Cao, J.J., Zhou, J.M., El-Haddad, I.,
1575 Huang, R.J., Ge, M.F., Tie, X.X., Prevot, A.S.H., Li, G.H., 2019. Wintertime secondary organic
1576 aerosol formation in Beijing-Tianjin-Hebei (BTH): contributions of HONO sources and
1577 heterogeneous reactions. *Atmospheric Chemistry and Physics* 19, 2343-2359.

1578 Xu, J., Zhang, Y.H., Wang, W., 2006. Numerical study on the impacts of heterogeneous reactions on
1579 ozone formation in the Beijing urban area. *Advances in Atmospheric Sciences* 23, 605-614.

1580 Xu, W., Yang, W., Han, C., Yang, H., Xue, X., 2021. Significant influences of TiO₂ crystal structures on
1581 NO₂ and HONO emissions from the nitrates photolysis. *Journal of Environmental Sciences* 102,
1582 198-206.

1583 Xue, C., Zhang, C., Ye, C., Liu, P., Catoire, V., Krysztofiak, G., Chen, H., Ren, Y., Zhao, X., Wang, J.,
1584 Zhang, F., Zhang, C., Zhang, J., An, J., Wang, T., Chen, J., Kleffmann, J., Mellouki, A., Mu, Y.,
1585 2020. HONO Budget and Its Role in Nitrate Formation in the Rural North China Plain.
1586 *Environmental Science & Technology* 54, 11048-11057.

1587 Xue, C.Y., Ye, C., Zhang, C.L., Catoire, V., Liu, P.F., Gu, R.R., Zhang, J.W., Ma, Z.B., Zhao, X.X.,
1588 Zhang, W.Q., Ren, Y.G., Krysztofiak, G., Tong, S.R., Xue, L.K., An, J.L., Ge, M.F., Mellouki, A.,
1589 Mu, Y.J., 2021. Evidence for Strong HONO Emission from Fertilized Agricultural Fields and its
1590 Remarkable Impact on Regional O₃ Pollution in the Summer North China Plain. *ACS Earth Space*
1591 *Chem.* 5, 340-347.

1592 Yang, K., Kong, L., Tong, S., Shen, J., Chen, L., Jin, S., Wang, C., Sha, F., Wang, L., 2021a. Double
1593 High-Level Ozone and PM_{2.5} Co-Pollution Episodes in Shanghai, China: Pollution Characteristics
1594 and Significant Role of Daytime HONO. *Atmosphere* 12, 557.

1595 Yang, W., Han, C., Yang, H., Xue, X., 2018. Significant HONO formation by the photolysis of nitrates
1596 in the presence of humic acids. *Environ Pollut* 243, 679-686.

Formatted: Subscript

1597 Yang, W., Han, C., Zhang, T., Tang, N., Yang, H., Xue, X., 2021b. Heterogeneous photochemical
1598 uptake of NO₂ on the soil surface as an important ground-level HONO source. *Environ. Pollut.*
1599 271, 116289.

1600 Ye, C., Gao, H., Zhang, N., Zhou, X., 2016a. Photolysis of Nitric Acid and Nitrate on Natural and
1601 Artificial Surfaces. *Environmental Science & Technology* 50, 3530-3536.

1602 Ye, C., Zhang, N., Gao, H., Zhou, X., 2017. Photolysis of Particulate Nitrate as a Source of HONO and
1603 NO_x. *Environmental Science & Technology* 51, 6849-6856.

1604 [Ye, C., Zhou, X., Pu, D., Stutz, J., Festa, J., Spolaor, M., Cantrell, C., Mauldin, R.L., Weinheimer, A.,
1605 Haggerty, J., 2015. Comment on “Missing gas-phase source of HONO inferred from Zeppelin
1606 measurements in the troposphere”. *Science* 348, 1326-d.](#)

1607 [Ye, C., Zhou, X., Pu, D., Stutz, J., Festa, J., Spolaor, M., Tsai, C., Cantrell, C., Mauldin, R.L., 3rd,
1608 Campos, T., Weinheimer, A., Hornbrook, R.S., Apel, E.C., Guenther, A., Kaser, L., Yuan, B., Karl,
1609 T., Haggerty, J., Hall, S., Ullmann, K., Smith, J.N., Ortega, J., Knote, C., 2016b. Rapid cycling of
1610 reactive nitrogen in the marine boundary layer. *Nature* 532, 489-491.](#)

1611 [Zaveri, R.A., Easter, R.C., Fast, J.D., Peters, L.K., 2008. Model for Simulating Aerosol Interactions
1612 and Chemistry \(MOSAIC\). *J Geophys Res-Atmos* 113. doi:10.1029/2007JD008782.](#)

1613 Zhang, H.L., Li, J.Y., Ying, Q., Yu, J.Z., Wu, D., Cheng, Y., He, K.B., Jiang, J.K., 2012. Source
1614 apportionment of PM_{2.5} nitrate and sulfate in China using a source-oriented chemical transport
1615 model. *Atmospheric Environment* 62, 228-242.

1616 Zhang, J., An, J., Qu, Y., Liu, X., Chen, Y., 2019a. Impacts of potential HONO sources on the
1617 concentrations of oxidants and secondary organic aerosols in the Beijing-Tianjin-Hebei region of
1618 China. *The Science of the total environment* 647, 836-852.

1619 Zhang, J., Chen, J., Xue, C., Chen, H., Zhang, Q., Liu, X., Mu, Y., Guo, Y., Wang, D., Chen, Y., Li, J.,
1620 Qu, Y., An, J., 2019b. Impacts of six potential HONO sources on HO_x budgets and SOA formation
1621 during a wintertime heavy haze period in the North China Plain. *The Science of the total
1622 environment* 681, 110-123.

1623 Zhang, J., Guo, Y., Qu, Y., Chen, Y., Yu, R., Xue, C., Yang, R., Zhang, Q., Liu, X., Mu, Y., Wang, J., Ye,
1624 C., Zhao, H., Sun, Q., Wang, Z., An, J., 2020a. Effect of potential HONO sources on peroxyacetyl
1625 nitrate (PAN) formation in eastern China in winter. *Journal of Environmental Sciences* 94, 81-87.

1626 Zhang, J., Ran, H., Guo, Y., Xue, C., Liu, X., Qu, Y., Sun, Y., Zhang, Q., Mu, Y., Chen, Y., Wang, J., An,
1627 J., 2022. High crop yield losses induced by potential HONO sources — A modelling study in the
1628 North China Plain. *Science of The Total Environment* 803, 149929.

1629 Zhang, L., Wang, T., Zhang, Q., Zheng, J.Y., Xu, Z., Lv, M.Y., 2016. Potential sources of nitrous acid
1630 (HONO) and their impacts on ozone: A WRF-Chem study in a polluted subtropical region. *J
1631 Geophys Res-Atmos* 121, 3645-3662.

1632 Zhang, N., Zhou, X.L., Shepson, P.B., Gao, H.L., Alaghmand, M., Stirn, B., 2009. Aircraft
1633 measurement of HONO vertical profiles over a forested region. *Geophysical Research Letters* 36.
1634 doi:10.1029/2009GL038999.

1635 Zhang, Q., Geng, G., 2019. Impact of clean air action on PM_{2.5} pollution in China. *Science China Earth
1636 Sciences* 62, 1845-1846.

1637 Zhang, S., Sarwar, G., Xing, J., Chu, B., Xue, C., Sarav, A., Ding, D., Zheng, H., Mu, Y., Duan, F., Ma,
1638 T., He, H., 2021. Improving the representation of HONO chemistry in CMAQ and examining its
1639 impact on haze over China. *Atmospheric Chemistry and Physics* 21, 15809-15826.

1640 Zhang, W., Tong, S., Ge, M., An, J., Shi, Z., Hou, S., Xia, K., Qu, Y., Zhang, H., Chu, B., Sun, Y., He,

Formatted: Subscript

1641 H., 2019c. Variations and sources of nitrous acid (HONO) during a severe pollution episode in
1642 Beijing in winter 2016. *The Science of the total environment* 648, 253-262.

1643 Zhang, W.Q., Tong, S.R., Jia, C.H., Wang, L.L., Liu, B.X., Tang, G.Q., Ji, D.S., Hu, B., Liu, Z.R., Li,
1644 W.R., Wang, Z., Liu, Y., Wang, Y.S., Ge, M.F., 2020b. Different HONO Sources for Three Layers
1645 at the Urban Area of Beijing. *Environmental science & technology* 54, 12870-12880.

1646 [Zhao, H., Zhang, Y., Qi, Q., Zhang, H., 2021. Evaluating the Impacts of Ground-Level O₃ on Crops in](#)
1647 [China. *Current Pollution Reports* 7, 565-578.](#)

1648 Zheng, H., Song, S., Sarwar, G., Gen, M., Wang, S., Ding, D., Chang, X., Zhang, S., Xing, J., Sun, Y.,
1649 Ji, D., Chan, C.K., Gao, J., McElroy, M.B., 2020. Contribution of Particulate Nitrate Photolysis to
1650 Heterogeneous Sulfate Formation for Winter Haze in China. *Environmental Science &*
1651 *Technology Letters* 7, 632-638.

1652 Zhou, X., Gao, H., He, Y., Huang, G., Bertman, S.B., Civerolo, K., Schwab, J., 2003. Nitric acid
1653 photolysis on surfaces in low-NO_x environments: Significant atmospheric implications.
1654 *Geophysical Research Letters* 30. doi:10.1029/2003GL018620.

1655 Zhu, C., Xiang, B., Zhu, L., Cole, R., 2008. Determination of absorption cross sections of
1656 surface-adsorbed HNO₃ in the 290–330 nm region by Brewster angle cavity ring-down
1657 spectroscopy. *Chemical Physics Letters* 458, 373-377.

1658 Zhu, Y.W., Liu, W.Q., Fang, J., Xie, P.H., Dou, K., Qin, M., Si, F.Q., 2011. Monitoring and Analysis of
1659 Vertical Profile of Atmospheric HONO, NO₂ in Boundary Layer of Beijing. *Spectroscopy and*
1660 *Spectral Analysis* 31, 1078-1082.

1661

Formatted: Subscript